A novel signaling role for nestin in regulating growth cone morphology via the cdk5 substrate DCX

Authors:
Christopher J. Bott[1], Jason M. Keil[2#], Lloyd P. McMahon[1#], Chan Choo Yap[1], Kenneth Y. Kwan[2], Bettina Winckler[1,3].

Addresses:
[1]Department of Cell Biology, University of Virginia, 1340 Jefferson Park Avenue, Pinn Hall Room 3226, Charlottesville, VA 22908, USA.
[2]Department of Human Genetics, University of Michigan, Ann Arbor, MI 48109
[3]Corresponding author:
Bettina Winckler (ORCID 0000-0002-7924-9313). Phone: (434)924-5528. E-mail: BWinckler@virginia.edu
[#] These authors contributed equally.

Condensed Title:
Nestin regulates DCX phosphorylation in neurons

Summary:
Bott et al. discovers a new mechanism by which the intermediate filament protein nestin regulates growth cones: Nestin complexes with the lissencephaly-linked protein DCX and potentiates its cdk5-mediated phosphorylation. Nestin thus regulates growth cone morphology in a DCX-dependent manner.

Abstract
Nestin, an intermediate filament protein widely used as a marker of neural progenitors, was recently found to be expressed in developing neurons where it regulates growth cone morphology. Nestin, which is known to bind the active cdk5/p35 kinase, additionally affects responses to axon guidance cues upstream of cdk5. Changes in growth cone morphology require rearrangements of cytoskeletal elements, but the roles of intermediate filament proteins in this process are poorly understood. Here, we investigated the molecular mechanism by which nestin affects growth cone morphology. We found that nestin specifically interacts with the Lissencephaly-linked microtubule-binding protein doublecortin (DCX). Nestin facilitates phosphorylation of DCX by cdk5/p35 through a scaffolding mechanism, but the phosphorylation of other cdk5 substrates is not affected. Lastly, we show that nestin's effects on growth cone morphology are DCX-dependent, thus demonstrating a functional role for the DCX-nestin complex in neurons. We propose that nestin changes growth cone behavior by regulating the intracellular kinase signaling environment in developing neurons.

Introduction

Correct wiring of the brain during development requires the targeting of growing axons to their future target fields. The outgrowth of axons is driven by the growth cone (GC) which is an actin- and microtubule (MT)-rich motile structure at the tip of growing axons (Menon & Gupton, 2016; Miller & Suter, 2018). GC motility is closely linked to the lengthening of axons (i.e. growth). GCs also serve as sensory devices and respond directionally to a large number of extracellular guidance cues that are precisely expressed in the developing brain in time and space (Petrovic & Schmucker, 2015; Yamamoto, Tamada, & Murakami, 2003). Guidance cues either attract or repel growth cones via specific receptors to achieve guided growth for development of proper circuitry (Dent, Gupton, & Gertler, 2011). Signaling elicited by guidance cues results in local downstream signaling responses which eventually result in rearrangement of the GC cytoskeleton to give directional growth (Vitriol & Zheng, 2012). The changes in GC behavior are mediated by a number of guidance cue-activated kinases and their downstream substrates, which include membrane and cytoskeleton regulators (Dent et al., 2011). Phosphorylation of cytoskeleton-associated proteins thus is a major mechanism by which the cell interprets incoming guidance cue information and converts it into morphological rearrangements of the GC for directed axon growth.

Most work on the cytoskeleton of axonal GCs has focused on actin filaments and MTs (Geraldo & Gordon-Weeks, 2009; Kapitein & Hoogenraad, 2015; Tamariz, Varela-echavarría, & Greer, 2015; Yamada, Spooner, & Wessells, 1970). Distinct roles for the third main cytoskeletal filament system, the intermediate filaments (IFs), during early axon formation and GC guidance in the developing brain are not as extensively studied. IFs are sparsely expressed in growing axons compared to mature axons (Benson, D. L., Mandell J. W., Shaw G., 1996; Brown, 2013; Chang & Goldman, 2004; K. Pennypacker, I. Fischer, 1991; Uchida & Brown, 2004; L. Wang, Ho, Sun, Liem, & Brown, 2000). Once axons reach their targets, the neurofilament class of IFs (NF-L, NF-M, and NF-H) are upregulated, in roughly sequential order as listed (Laser-Azogui, Kornreich, Malka-Gibor, & Beck, 2015; Nixon & Shea, 1992; Yabe et al., 2003). Neurofilaments ultimately fill most of the axon along its length and have important structural roles in mature axons to maintain axon caliber (Lariviere & Julien, 2003; Rao et al., 2003; Z. Xu, J. Marszalek, M. Lee, P. Wong, J. Folmer, T. Crawford, ST. Hsieh, J. Griffin, 1996).

We recently discovered that the atypical IF protein nestin regulates GC morphology and responsiveness to the repellent guidance cue Sema3a (Bott et al., 2019). Nestin is highly expressed in neuronal progenitor cells and is used as a marker to label them. We found that lower levels of nestin protein are present in post-mitotic cortical neurons. Nestin accumulates strikingly in the distal axon “wrist” region, the transitional zone between the axon shaft and the growth cone, and extends into the central domain of axonal GCs, but is not detectable in future dendrites. We showed that downregulation of nestin increases GC size and blunts sensitivity to the cdk5-dependent axonal guidance cue Sema3a (Bott et al., 2019). Our previous study (Bott et al., 2019) thus was the first to discover a role for nestin in neurons, but the molecular pathways by which nestin affects growth cones remained unknown. Little is known about nestin function generally, even in progenitor cells where it is highly expressed. In other cell types, nestin has been shown to affect the activity of cdk5. In neuromuscular junction (NMJ) development, for example, nestin deletion phenocopies cdk5 deletion or

treatment with the cdk5 inhibitor roscovitine by altering levels and localization of cdk5 activity (Lin et al., 2005; Yang et al., 2011). The physiological substrates of cdk5 affected by nestin at the NMJ are still unknown. In this work, we discovered a neuronal nestin-regulated cdk5 substrate, namely DCX, and show that nestin's effect on GC morphology is DCX-dependent.

DCX is a multifunctional cytosolic protein expressed in growing neurons. Mutations in human DCX cause lissencephaly, a disease characterized by defects in neuronal migration and axon outgrowth that results in profound cortical malformations (Bahi-Buisson et al., 2013). Patients exhibit intellectual disability and intractable epilepsy and often die young. *In vitro*, DCX promotes MT assembly, and DCX-bound MTs are less dynamic (Moores et al., 2004). In addition, expression of DCX in heterologous cells leads to formation of bundled MTs which are very stable (Ge et al., 2006; Gleeson, Peter T, Flanagan, & Walsh, 1999; Moslehi, Ng, & Bogoyevitch, 2017; Sapir et al., 2000; Tanaka, Serneo, Tseng, et al., 2004; Tsukada, Prokscha, Ungewickell, & Eichele, 2005; Yap et al., 2018, 2012). DCX is widely regarded primarily as a MT-associated protein, but DCX can also associate with endosomal machinery directly (G Friocourt et al., 2001; Yap et al., 2012), and with actin filaments indirectly through the actin binding protein spinophilin (SPN)(Tsukada, Prokscha, & Eichele, 2006; Tsukada, Prokscha, Oldekamp, & Eichele, 2003; Tsukada et al., 2005). Furthermore, recent evidence demonstrated that different DCX patient mutations cause distinct disruptions of cellular machinery (Fu et al., 2013; Yap et al., 2018, 2016), suggesting that non-MT interactions of DCX contribute to its function and can cause pathology when disrupted.

In neurons, DCX is not found along all MTs evenly but is enriched at the distal regions of axons and dendrites (Gaëlle Friocourt et al., 2003; Schaar, Kinoshita, & McConnell, 2004),and is thought to coordinate actin in the distal GC with MTs in the axon shaft (Bielas et al., 2007). DCX has well documented effects on MT morphology of growth cones (Bielas et al., 2007; Jean, Baas, & Black, 2012), affects corpus callosum formation in mice and humans (Bahi-Buisson et al., 2013; Bielas et al., 2007; C. Kappeler, M. Dhenain, F. Phan Dinh Tuy, Y. Saillour, S. Marty, C. Fallet-Bianco, I. Souville, E. Souil, JM. Pinard, G. Meyer, F. Encha-Razavi, A. Volk, C. Beldjord, J. Chellly, 2007; Fu et al., 2013) , and operates downstream of at least one guidance cue in culture, namely netrin (Fu et al., 2013). Multiple kinases regulate DCX phosphorylation which affects where and how DCX associates with MTs (Schaar et al., 2004; Tanaka, Serneo, Tseng, et al., 2004). One important DCX kinase is the serine/threonine kinase cdk5 (Tanaka, Serneo, Tseng, et al., 2004) - a cytoskeletal remodeling kinase particularly highly expressed in neurons (Nishimura, Shikanai, Hoshino, Ohshima, & Nabeshima, 2014; Xie, Samuels, & Tsai, 2006). Cdk5 is related to the mitotic cyclin-dependent kinases (CDKs), but is regulated by p35, not by cyclins and is largely absent from mitotic cells (Lew et al., 1994; Lew, Winkfein, Paudel, & Wang, 1992; Meyerson et al., 1992; Tsai, Delalle, Caviness, Chae, & Harlow, 1994). It plays critical roles in neurodevelopment as cdk5 KO mice have profound disturbances in cortical development (Shah & Lahiri, 2014; Shinmyo et al., 2017; Shupp, Casimiro, & Pestell, 2017). Similarities between the brains of cdk5 knockout mice and human DCX patient brains originally suggested a possible role for cdk5 in regulating DCX function (Tanaka, Serneo, Tseng, et al., 2004). Phosphorylation of DCX by cdk5 indeed

decreases the affinity of DCX for MTs and thus leads to decreased MT stability and increased MT dynamics (Bielas et al., 2007; Tanaka, Serneo, Higgins, et al., 2004). There are several known serine/threonine residues in DCX which can be phosphorylated by cdk5, but the precise effect on DCX function for each of these phosphorylation events is not known (Gdalyahu et al., 2004; Graham et al., 2004; Moslehi et al., 2017; Reiner et al., 2004; Singh et al., 2012).

In this work, we propose a novel mechanism by which nestin affects growth cone morphology. We identify DCX as a novel nestin-associated protein and demonstrate that cdk5 potently phosphorylates nestin-scaffolded DCX. Interestingly, nestin specifically promotes cdk5 phosphorylation of DCX, but not of other cdk5 substrates. Nestin thus regulates downstream signaling of the neuronal kinase cdk5 specifically by scaffolding DCX together with cdk5. In fact, we show that nestin's effects on growth cone morphology are DCX-dependent, thus demonstrating a functional role for the DCX-nestin complex in neurons.

Results

Nestin interacts specifically with DCX

Our recent work (Bott et al., 2019) discovered an unexpected role for nestin in axonal growth cones: downregulation of nestin increases GC size and decreases Sema3a sensitivity. Since nestin binds the cdk5 activator p35 (Sahlgren et al., 2003, 2006; Yang et al., 2011), and cdk5 inhibition inhibits the effect of nestin-associated Sema3a-mediated collapse in neurons (Bott et al., 2019), we reasoned that one or more cdk5 substrates might be involved in mediating the nestin-dependent changes in GCs. In order to unravel the molecular machinery by which nestin affects cdk5 dependent processes in neurons, we tested whether any of the known neuronal cdk5 substrate interacted with nestin by co-immunoprecipitation (co-IP). We focused on six cdk5 substrates known to be phosphorylated downstream of Sema3a signaling.

First, we used overexpression in heterologous cells (HEK293) to test if candidate proteins formed a complex with nestin. We co-transfected Nestin-myc or myc-empty vector (EV-negative control) with each GFP-tagged substrate (Doublecortin (DCX), Doublecortin like Kinase 1 (DCLK1), Collapsin Response Mediator Protein 2 (CRMP2), Tau, Drebrin, and Focal Adhesion Kinase (FAK)) individually in HEK293 cells followed by cell lysis and anti-myc tag immunoprecipitation (Fig. 1A). The efficiency of co-IP with nestin-myc was assessed for each GFP-tagged substrate by densitometry analysis as a ratio of immunoprecipitated protein to the total amount of protein in the corresponding input. Only GFP-DCX significantly co-immunoprecipitated with nestin-myc (Fig. 1A, A'). In order to test if the ability of DCX and nestin to form a complex affected their respective cellular localizations, we transfected COS-7 cells which are well spread and have spatially resolvable MT and vimentin IF filament systems. As shown previously by us and others, GFP-DCX decorates MTs (Ge et al., 2006; Gleeson et al., 1999; Moslehi et al., 2017; Sapir et al., 2000; Tsukada et al., 2005; Yap et al., 2018, 2012), but is not associated with vimentin (Fig. S1A). Conversely, Nes-myc colocalized with endogenous vimentin in the absence of DCX (Fig. S1B), but was recruited to DCX-decorated MT bundles when DCX was co-expressed (Fig. S1C). When a different MAP, YFP-tau, was expressed instead of DCX, nestin remained associated with vimentin IFs (Fig. S1D).

Other IFs, like α-internexin (INA), did not associate with DCX-MT bundles (Fig. S1E). We thus identified a novel complex of nestin and DCX.

To determine if the nestin-DCX complex occurred endogenously in the relevant tissue, embryonic rodent brain was subjected to IP with either nestin (Fig. 1B) or DCX (Fig. 1B') antibodies and compared to non-immune IgG. An endogenous complex of nestin and DCX was recovered for both IPs. IP with nestin antibody resulted in efficient co-IP of DCX. In contrast, relatively low amounts of nestin were recovered in the IP with a DCX antibody, but when compared to the known DCX interacting protein SPN (a positive control), similar levels of co-IP efficiency were detected. This is likely due to the fact that DCX is a multifunctional protein which has a multitude of binding interactions which might be mutually exclusive. The non-interacting protein drebrin was not detectable in the co-IP, serving as a negative control. In agreement with these findings, we also found nestin by mass spectrometry in DCX IPs of embryonic rat brain (Yap CC, unpublished data).

In order to test if the DCX-nestin complex was present in neurons (as opposed to in another cell type present in brain lysates), we repeated the IP with lysates from E16 cortical neurons cultured for one day in vitro (DIV1). Indeed, nestin could be seen to co-IP with DCX (Fig. 1C) in DIV1 cortical cultures. As a negative control, we carried out IPs from neuronal cultures prepared from DCX KO E16 cortex. The DCX KO neurons expressed similar levels of nestin as WT cultures, but no nestin was detected in the DCX IP (Fig. 1C). We thus discovered a novel endogenous complex of DCX and the intermediate filament protein nestin in immature cortical neurons.

Nestin and DCX co-localize in the distal axon of cortical neurons *in vitro* and *in vivo*

We previously described a striking localization of nestin in the distal axon of cultured E16 mouse cortical neurons at 1 DIV that was rapidly lost as the neurons matured (Bott et al., 2019). DCX is enriched in the distal axon, but is also present in dendrites (Gaëlle Friocourt et al., 2003; Schaar et al., 2004). Simultaneous staining with antibodies against DCX and nestin revealed co-localization in the distal axon (Fig. 2A; arrowhead), but not in dendrites. Enhanced resolution microscopy of the distal axon showed that nestin co-distributed with DCX in the "wrist" region of the axonal growth cone (Fig. 2B) and appeared to be filamentous. Some fraction of nestin also extended past the "wrist" into the central domain and even into some of the proximal filopodia of the growth cone.

We previously showed nestin immunostaining in E16.5 mouse cortex in axon fascicles in the intermediate zone (IZ) which are interwoven among highly expressing radial glial processes (Bott et al., 2019). However, we were unable to discern single axons *in vivo*, let alone single growth cones, due to the high density of axons in the IZ. In order to visualize nestin localization in individual developing axons *in vivo*, we utilized *in utero* electroporation (IUE) to sparsely label individual neurons by CRISPR/Cas9 genome editing (Fig. S2A). Tagging endogenous β-actin with 3xHA tags enabled us to label the actin cytoskeleton of developing neurons including the growth cone. Three days after IUE, brains were fixed, sectioned and immunostained for the HA-tag in combination with staining for DCX and nestin (Fig. 2C). This technique introduced the HA tag into a small number of newly born neurons, which were scattered throughout the IZ and cortical plate (CP) at multiple stages of maturation. We expected to find nestin-

positive axon tips in only a subset of labeled neurons (Bott et al., 2019) and therefore focused on neurons that were migrating though the IZ and had not yet reached the cortical plate. These neurons are less mature and still in the early stage of axon extension (Namba et al., 2014; Sakakibara & Hatanaka, 2015) and thus most analogous to the young neurons we used in culture. One such neuron (soma marked with red arrowhead, axon tip marked with white arrowhead) is shown in Fig. 2C'. The nestin staining pattern in the IZ consists of bright radial staining of the radial glial processes and fainter staining of axons running parallel to the ventricular surface, as we showed previously (Bott et al., 2019). The sparse labeling provided by the HA-tag knock in strategy thus allowed us to identify individual neurons which had nestin-positive growth cones. A high magnification of a single section of a z-stack shows an example of nestin staining that clearly localizes within the distal region of the extending axon (Fig. 2C''). Orthogonal projections of the z-stack were used to allow for visualization of nestin within the HA-positive axon (Fig. 2C'''). Enhanced resolution Airyscan confocal imaging of the same growth cone in the same z-plane allows for better appreciation of the axonal nestin (Fig. 2C''''). Nestin in distal axons is thus also observable *in vivo* and thus mirrors what was seen in culture (Bott et al., 2019). In addition, nestin was seen primarily in the smaller, more compact GCs of younger neurons whose cell bodies had not yet reached the cortical plate (CP). The growth cones of longer axons (presumably belonging to more mature neurons) did not have detectable nestin enrichment in the growth cones and were larger in size (Fig. S2B).

<u>Nestin promotes phosphorylation of DCX by cdk5.</u>

Because nestin is a known cdk5 modulator, and DCX is a known cdk5 substrate, we sought to determine whether nestin affected DCX phosphorylation by cdk5. To this end, we utilized an "in-cell" phosphorylation assay in transfected HEK293 cells (Fig. 3A). HEK293 cells endogenously express cdk5, but not the cdk5 activator p35. They thus have minimal cdk5 activity under basal conditions. Cdk5 phosphorylation of DCX can be detected with a phosphospecific antibody against serine at position 297 (S297), which has been shown to be a major cdk5 site of DCX in neurons and is diminished in cdk5 null mice brains (Tanaka, Serneo, Tseng, et al., 2004). An antibody against pS334, a known JNK site, was used as a negative control. We expressed p35 with or without nestin-myc and determined the levels of pS297-DCX. When p35 was expressed with GFP-DCX in the absence of nestin-myc, we surprisingly did not get increased phosphorylation of DCX at S297. When p35 was co-expressed with nestin-myc, in contrast, we saw a significant increase in pS297-DCX levels (Fig. 3A', grey bars).

Interestingly, nestin co-expression with p35 consistently resulted in an increase in total DCX levels, which is likely due to stabilization of DCX protein in its phospho-form. This has been reported for other cdk5 substrates (Eva & Fawcett, 2014; Grant et al., 2015; Kreis et al., 2019; Poppek et al., 2006), and we ourselves also saw it with tau and Crmp2 (see Fig. 4). For quantification, we thus ratio'ed the phospho-epitope signal to total expression of GFP-DCX (Fig. 3A'). P35 was also stabilized by nestin co-expression in our hands, as was reported before (Sahlgren et al., 2003, 2006) (see Fig. 4 for additional experiments).

Multiple residues in addition to S297 are phosphorylated by cdk5 on DCX, but specific antibodies to detect these phosphorylation events are not available. We

obtained another antibody, which recognizes the general "K/H pSP" phospho-epitope consensus site for cdk's to confirm our results with the pS297 antibody. GFP-DCX was precipitated from lysates with GFP-trap agarose beads to separate DCX from other reactive endogenous cdk substrates in this experiment. Similar to our results using the anti-pS297DCX antibody, a significant nestin-dependent increase in cdk5 phosphorylation of DCX could also be seen with this cdk phospho-substrate antibody (Fig. S3A and quantified in S3A').

In contrast to S297, the phosphorylation of S334 by JNK was not changed by co-expression of nestin (Fig. 3A,A', red bars). The dependence of the pS297-DCX and pS334-DCX antibodies on phosphorylation was confirmed by co-expression of SPN (Fig. 3 A,A') which is a known PP1 phosphatase scaffold and promotes dephosphorylation of both the cdk5 and JNK sites of DCX (Bielas et al., 2007; Shmueli et al., 2006; Tsukada et al., 2006). In addition, a different neuronal IF, INA, which did not bind DCX (see Fig. 5B below and S1E), did not promote DCX phosphorylation by p35/cdk5, arguing for a specific enhancement of cdk5 phosphorylation by nestin (Fig. 3A,A'). We further tested that S297-DCX phosphorylation was in fact occurring via cdk5 and not via other endogenous kinases present in COS-7 cells. The cdk5 inhibitor roscovitine reduced pS297DCX phosphorylation, but neither SP600125 (JNK inhibitor) nor Ro3306 (cdk1/cdc2 inhibitor with minimal cross-reactivity with cdk5) changed the pS297-DCX levels (Fig. 3B, 3B'), supporting previous literature that S297 is a cdk5 site on DCX (Tanaka, Serneo, Tseng, et al., 2004).

Lastly, we wanted to determine if S297 was a relevant cdk5 epitope in cortical neurons. Since S297-DCX phosphorylation has been reported to be induced by Sema3a in DRG neurons (Ng et al., 2013), we treated DIV1 E16 cortical mouse neurons with vehicle or 1 nM Sema3A for 5, 15, or 30 minutes. We could detect phosphorylation of the S297-DCX epitope in neurons, which was significantly increased after Sema3a treatment (Fig. S3B,B'). The JNK site pS334 was not increased after Sema3a treatment (Fig. S3B,B'). pS297DCX, but not pS334DCX levels, were reduced by roscovitine, consistent with activation of cdk5 downstream of Sema3a (Fig. S3B").

<u>Nestin specifically augments cdk5-kinase activity towards DCX, but not other cdk5 substrates.</u>

Is nestin universally increasing cdk5/p35 activity? If cdk5 activity were globally upregulated by nestin, we would expect that other known cdk5 substrates would also show increased phosphorylation in the presence of nestin, even if these substrates did not interact with nestin themselves. Commercially available phospho-specific antibodies for Crmp2, tau, and FAK were used to test for nestin modulation of cdk5 phosphorylation on these substrates (Fig. 4). In contrast to DCX, Crmp2, tau, and FAK showed p35-dependent increases in phosphorylation, but none showed further increases in phosphorylation when nestin was co-expressed with p35 (Fig. 4A-C). As a control, we utilized an antibody to a phospho-tyrosine residue on FAK. As expected, pY397 FAK was not affected in any condition (Fig. 4D). We included DCX in parallel again in these experiments and observed the same pattern as in Fig. 3: nestin enhances cdk5-mediated phosphorylation of pS297-DCX, but not of pS334-DCX (Fig. 4E,F). We note that there was basal phosphorylation for some of these substrates even

in the absence of overexpressed p35, which may be due to activity of other kinases in 293 cells.

What is the mechanism for nestin-mediated enhancement of cdk5 phosphorylation of DCX? As mentioned above, we observed that nestin expression resulted in stabilization of p35 (Fig. 3), as previously reported (Pallari, Lindqvist, Torvaldson, Ferraris, & He, 2011; Sahlgren et al., 2003, 2006; Yang et al., 2011). This was proposed to be a mechanism by which nestin promoted cdk5 activity, as it is reasonable to suspect that more activator results in more cdk5 activity. To test this model directly, we expressed increasing amounts of p35 in HEK293 cells by increasing the amount of p35 plasmid used in the transfection from 1 to 4 µg. We see an increased amount of p35 expressed with more p35 plasmid used (Fig. 4G). We could thus directly compare the levels of pS297-DCX at similar p35 levels with or without nestin. Even with similar levels of p35, levels of pS297-DCX are not increased in the absence of nestin (Fig. 4G,G'). This demonstrates that the increased p35 levels are not sufficient to account for the increased DCX phosphorylation by cdk5 observed with nestin co-expression. This is in agreement with our evidence that nestin only affects phosphorylation of cdk5 substrates that it interacts with (i.e. DCX), but not non-nestin binding substrates (Fig. 4A-F). Nestin thus did not increase global cdk5 activity in the cell, but selectively increased cdk5 activity towards DCX.

Nestin scaffolds cdk5/p35 for DCX phosphorylation

We next asked how nestin specifically increases phosphorylation of DCX? We know that nestin interacts with the cdk5/p35 heterodimer complex (Sahlgren et al., 2003; Yang et al., 2011). Thus we hypothesized that nestin acts to scaffold the active kinase (cdk5/p35) with one of its substrates (DCX) by binding to both proteins simultaneously (see diagram top panel Fig. 5A). We know that typically an interaction between a kinase and substrate is transient, and phosphorylation of the substrate can result in dissociation of the kinase from the substrate (see diagram top panel Fig. 5A) (E. Goldsmith, R. Akella, X. Min, T. Zhou, 2007; Manning & Cantley, 2002). Kinases which have had the catalytic residues mutated to be inactive ("kinase dead" KD), can form more stable complexes with their substrates. If this modification does not interfere with kinase-substrate binding per se, then the substrate will be "trapped" by the kinase and will result in an increase in substrate-kinase co-IP efficiency (bottom panel Fig. 5A). In order to test if nestin had this type of relationship with DCX, we compared the extent of DCX-nestin complex formation (by nestin-myc IP) in cells co-expressing HA-cdk5-WT or HA-cdk5-Kinase dead (KD)(D145N)(Fig. 5B). We could co-IP significantly more DCX with nestin when the substrate-trapping cdk5-KD was coexpressed, compared to a low co-IP efficiency with cdk5-WT (Fig. 5B'). As a negative control, co-expression of INA-myc, which does not interact with p35 or DCX, resulted in only background levels of GFP-DCX co-IP in all conditions (Fig. 5B). These results suggested that nestin was acting as a scaffold between cdk5 and DCX. To more directly test this idea, we pulled down the kinase complex via p35 IP, to test for differences in DCX co-IP in the absence or presence of nestin (Fig. 5C). We again utilized the substrate-trapping kinase-dead (KD) cdk5 mutant, which results in stable complex formation (Fig. 5A,B). We find that nestin co-expression significantly increased the amount of DCX recovered in the co-IP by a p35 antibody, suggesting a complex of p35-cdk5KD with DCX and nestin (Fig. 5C,

5C'). Nestin did not affect cdk5/p35 heterodimer formation, as there was not a significant difference (p=0.88, n=3) in the amount of cdk5 recovered by p35 IP in the presence or absence of nestin (not shown). Thus, we propose that nestin acts as a selective scaffold, which can bind to cdk5/p35 and DCX simultaneously, and this results in increased efficiency of WT cdk5 to phosphorylate DCX (Fig. 5D). Dephosphorylation of DCX was shown by others (Bielas et al., 2007; Shmueli et al., 2006) (and confirmed by us in Fig. 3A,A') to be dependent on the recruitment of PP1 to DCX by the actin binding protein SPN. Thus, we propose that the level of DCX phosphorylation is determined by the balance between these opposing reactions, and that dephosphorylation would be more dominant when nestin is absent. We thus envision nestin to act like a "gain controller" in growth cones that sensitizes DCX to cdk5 phosphorylation.

<u>The T316D mutation in nestin affects p35 and DCX binding as well as DCX phosphorylation, but not incorporation into vimentin filaments.</u>

We previously showed that nestin expression is associated with small compact GCs and that nestin negative-neurons have larger GCs (Bott et al., 2019). Is the effect of nestin on GC morphology dependent on the scaffolding of cdk5/p35/DCX by nestin? To test this, we aimed to create nestin mutants that lack cdk5/p35 binding. Previous work showed that the threonine at position 316 site on nestin is an important regulatory site for p35 binding (Su et al., 2013; Yang et al., 2011). The T316 site can be phosphorylated, which affects binding to p35. The T316A phospho dead mutant had been shown to have increased binding to p35 in in vitro binding assays of purified recombinant protein (Yang et al., 2011). In addition to making the T316A phospho-dead nestin mutant, we created and characterized a phospho-mimetic mutant (T316D-Nes) with respect to p35 binding. To characterize p35 binding, we used a co-IP strategy similar to that used in Figure 1, by expressing WT or mutant nestin each with p35 in HEK293 cells, and subjected the lysates to anti-myc IP (Fig. 6A). In our hands, the T316A mutant had only a slight, insignificant, increase in p35 binding. T316D-Nes, on the other hand, co-IP'ed less p35. (Fig. 6A).

We then wanted to test if these nestin mutant proteins had altered ability to form a complex with DCX. We performed IPs with WT nestin or nestin mutants when GFP-DCX was expressed. Surprisingly, the T316D-Nes mutant also had decreased binding with DCX (Fig. 6A). We note that T316D-Nes was consistently present at lower levels in the lysates compared to WT nestin or T316A-Nes. This is not unexpected, as other studies have shown that phosphorylation of nestin leads to it degradation (Pallari et al., 2011; Sahlgren et al., 2003, 2006). Since variations in nestin expression levels make it harder to directly compare co-IP efficiency on western blots, we qualitatively determined if sufficient levels of T316D-Nes were present in our lysates to demonstrate known binding interactions. Since nestin forms heteropolymers with vimentin, we tested for co-IP of nestin WT or mutants with vimentin. The 316 site is just outside of the IF polymerization rod domain, so modification of this site is not expected to interfere with IF polymerization. We observed WT nestin, T316A-Nes, and T316D-Nes mutant co-IP'ing with vimentin effectively (Fig. 6A), arguing that they still form homo-oligomers/polymers with vimentin. In agreement, these mutants appeared to co-distribute with vimentin similarly to WT nestin in COS-7 cells (Fig. S4A-C). We thus

conclude that T316D-Nes binds less well to p35 and DCX whereas T316A-Nes still binds p35 and DCX, and that neither mutation grossly disrupted vimentin binding. In agreement with the co-IP studies, both WT nestin and T316A-Nes still showed association with GFP-DCX MT bundles in COS-7 cells, whereas T316D-Nes did not (Fig. S4D-F).

Our scaffolding hypothesis proposes physical associations between DCX, p35/cdk5, and nestin. We thus reasoned that a nestin mutant deficient in p35 and DCX binding should also be deficient in promoting cdk5-mediated phosphorylation of DCX. We tested if the pS297-DCX levels were altered in cells expressing WT or T316 nestin mutants (Fig. 6B). T316A-Nes + p35 resulted in increased phosphorylation of DCX similar to WT nestin + p35, whereas T316D-Nes + p35 did not result in increased phosphorylation of DCX (Fig. 6B, quantified in 6B'). This supports our scaffolding hypothesis, and we thus used the T316D-Nes mutant to test the role of the nestin-p35-DCX complex in neurons.

Binding to p35 and/or DCX is required for nestin's effect on growth cone size.

We previously reported that reducing neuronal nestin levels leads to larger GCs (Bott et al., 2019). How does overexpression of WT nestin or of T316 nestin mutants affect GC size? We expressed various myc-tagged constructs in cultured cortical neurons for 2 days along with GFP to allow for detection of transfected cells. At this stage, the majority of neurons are nestin-negative (Bott et al., 2019). Overexpression of WT nestin-myc resulted in statistically smaller GCs on axons (arrows) with fewer filopodia when compared to overexpression of INA-myc or myc-EV (Fig. 6C, C', C''). T316A-Nes, which retained binding to p35 and DCX (Fig. 6A) and resulted in WT levels of DCX phosphorylation (Fig. 6B), resulted in small GCs with fewer filopodia, similar to WT nestin (Fig. 6C). However, the T316D-Nes mutant, which did not interact with p35 or DCX (Fig. 6A) and did not result in increased DCX phosphorylation (Fig. 6B), did not significantly alter GC size or filopodia number (Fig. 6C, C', C''). Therefore, binding to p35 and/or DCX was required for nestin's effect on GC size.

Nestin does not have any effect on GC size in the absence of its downstream effector DCX.

Since nestin specifically bound to DCX and affected its phosphorylation, we hypothesized that the effects of nestin overexpression on GCs were dependent on DCX. Therefore, we predicted that nestin overexpression would not affect GCs in the absence of DCX. We thus tested if nestin affected the GC size in DCX null neurons and WT neurons differently. We utilized the nestin overexpression assay as above and compared nestin-myc overexpression to myc-EV and myc-INA. We again observed decreased axonal GC size (arrows) specifically with nestin-myc expression (Fig. 7A,B). However, in DCX null neurons, no decrease in GC size was seen with nestin-myc expression (Fig. 7). When GFP-DCX was reintroduced together with nestin-myc into DCX null neurons, the nestin effect on GC size was rescued (Fig. 7). We thus conclude that nestin acts via DCX to influence GC size.

Discussion

A number of IF subtypes are expressed in the brain, but their cell biological functions during development are incompletely understood (Yuan & Rao, 2012). One of the earliest expressed IFs in the developing brain is nestin, but little is known about nestin's function, even in NPCs where it is highly expressed (Mohseni et al., 2011; Park et al., 2010). We previously found that nestin protein expression persists at low levels in early neurons and that nestin expression influences growth cone size and responsiveness to Sema3a in a cdk5-dependent manner (Bott et al., 2019), but the molecular pathways for this phenotype were not known. Nestin is known to directly interact with the p35 subunit of the active cdk5 heterodimer. We thus hypothesized that nestin might also affect the activity of cdk5 in neurons, similarly to what occurs during neuromuscular junction development (Yang et al., 2011). Hence, we screened known neuronal cdk5 substrate cytoskeletal proteins for nestin binding and identified DCX as a novel nestin-associated protein. Mechanistically, we find that nestin promotes robust phosphorylation of DCX by cdk5/p35 and that DCX is required for the effects of nestin on GCs. In summary, our results uncover a novel signaling role for neuronal nestin in regulating GC morphology specifically via scaffolding the cdk5 substrate DCX.

<u>DCX is a substrate for nestin-scaffolded cdk5 in neurons.</u>

Earlier work identified nestin as a p35 binding protein and showed that nestin modulated both the level and localization of cdk5 activity in C2C12 myotubes (Yang et al., 2011). *In vivo*, nestin depletion phenocopies cdk5 deletion or roscovitine treatment in maintaining acetylcholine receptor clustering in agrin (AGD) mutants (Lin et al., 2005; Mohseni et al., 2011; Yang et al., 2011). However, the effect of nestin depletion on cdk5 activity (promoting or inhibiting) has varied between reports and assay systems and has been a point of contention (Huang, Wu, Shi, & Wu, 2017; Lindqvist et al., 2017; Pallari et al., 2011; Sahlgren et al., 2006; Women et al., 2017; Yang et al., 2011; Zhang et al., 2018). Since the relevant endogenous cdk5 substrate in myoblasts remains unknown, exogenous substrates (such as recombinant H1 histone) are commonly used for phosphorylation assays. It is unclear how phosphorylation of a nuclear substrate (H1 histone) can translate into measuring cytosolic cdk5 activity. The different interpretations are thus likely due to the use of exogenous substrates in the phosphorylation assays. Our work for the first time identifies a biologically relevant substrate for nestin-scaffolded cdk5, namely DCX (Fig. 3). If DCX is also the relevant substrate in myoblasts is not known, but it is intriguing that DCX null mice also have developmental defects at the neuromuscular junction, as do human lissencephaly patients with DCX mutations (Bourgeois et al., 2015). Our work suggests that nestin does not modulate cdk5/p35 kinase activity per se since nestin did not affect cdk5/p35 heterodimer formation and several other cdk5 substrates were not affected by nestin (Fig.4 and 5). Rather, we propose that in neurons nestin specifically increases cdk5-mediated DCX phosphorylation by providing a scaffold.

<u>DCX as a downstream effector of nestin: a model for regulation of GC size.</u>

How does nestin affect GC size via DCX? Three major processes are necessary for axon growth and guidance - protrusion, engorgement, and consolidation (Dent & Gertler, 2003). Protrusions towards positive guidance cues are mediated by actin-based

filopodia and lamella which serve as templates for subsequent MT infiltration and growth. These MTs stabilize the new actin-based structures and allow for transport of cell components through vesicular trafficking which leads to the filling and engorgement of the advancing growth cone. The absence of DCX results in decreased stability and extent of protruding MTs (Jean et al., 2012). Lastly, the proximal part of the growth cone is consolidated, and MTs are bundled into new axon shaft. MT-binding proteins play essential roles in regulating the assembly dynamics and bundling extent of MTs in a spatially regulated manner and are critical regulators of axon growth. Phosphorylation and dephosphorylation are known to spatially regulate the activities of many MAPs, including DCX. We propose that nestin affects GC size by promoting the phosphorylation of DCX in the distal axon. Dephosphorylation of DCX has already been implicated in the consolidation step of axon growth (Bielas et al., 2007). In particular, Bielas et al. (2007) showed that cdk5-mediated phosphorylation of DCX is reversed by the phosphatase PP1 which is scaffolded by the DCX-binding protein SPN (Tsukada et al., 2006). In extension of these earlier models, we propose that nestin scaffolds cdk5 and thereby promotes the phosphorylation of DCX - thus completing the regulatory cycle of DCX phosphorylation and dephosphorylation (Fig. 5D). The regulation of the phosphorylation of DCX is thus driven by the balance of nestin/cdk5/p35 to increase phosphorylation and SPN/PP1 to decrease it - perturbation of either process results in abnormal MT organization (Bielas et al., 2007; L. Dehmelt, 2007; Schaar et al., 2004). In our model, the level of phospho-DCX would be determined by the relative opposing activity of the two differently localized regulatory complexes (Fig. 5D).

On a molecular level, we predict that the presence of nestin would result in more pS297-DCX, which has a decreased affinity for MTs. We were unable to stain neurons with the pS297-DCX antibody reliably and could thus not test this idea directly. Since DCX binding to MTs stabilizes them (Moores et al., 2004), growth cones with more pS297-DCX may have intrinsically less stable and possibly less bundled MTs. This notion is consistent with previous findings that GC size reflects MT dynamics. For instance, smaller growth cones have intrinsically more dynamic MTs than larger growth cones (Kiss, Fischer, Kleele, Misgeld, & Propst, 2018). In addition, treatment with taxol, which stabilizes MTs, results in larger GCs (Gumy et al., 2013). Thus we propose that a smaller growth cone represents a GC with more robust kinase/phosphatase activity which would result in more rapid cytoskeletal dynamics, morphological turnover, and GC sculpting via changes in the phosphorylation of cytoskeletal associated proteins, including DCX. A smaller GC would thus correlate with a more robust response to a given relevant guidance cue as it is able to remodel the existing cytoskeleton more rapidly.

<u>A novel role for intermediate filaments in axon growth.</u>

IFs have previously not been thought to be important for axon formation, much less axon guidance. Early studies had concluded that IFs were absent from the most distal and peripheral regions of the growth cone, and thus were ruled out early on as relevant players in regulating axon targeting (Dent & Gertler, 2003). However, the higher resolution and more sensitive imaging methods used here (Fig. 2), reveal intermediate filaments in some peripheral regions of the GC, suggesting this question should be revisited. Additionally, it is also commonly thought that intermediate filaments

or neurofilaments do not affect axon guidance, because NF-deficient mice still develop axon tracts and do not have obvious neurological defects. NFL and NFM depletion results in significantly decreased caliber of axons, but interestingly also results in a non-significant, but consistent, 10-20% decrease in axon number (Elder et al., 1998; Perrot, Berges, Bocquet, & Eyer, 2008; Zhu, 1997). Interestingly, a study in Xenopus using acute inactivation of neurofilaments in early Xenopus neurons via microinjection of anti-NFM antibodies found that axons spent more time idling, resulting in a slower overall growth rate (Lin & Szaro, 1996; Szaro, Grant, Lee, & Gainer, 1991; W. Lin, 1995; Walker, Yoo, Undamatla, & Szaro, 2001). In addition, a series of studies by Shea and colleagues found that depletion of IFs and NFs decreased neurite formation in neuroblastoma cells (Boyne, Fischer, & Shea, 1996; Dubey et al., 2004; Lee & Shea, 2014; Shea & Beermann, 1999; Shea, Beermann, & Fischer, 1993). It remains thus an open question whether or not some intermediate filament proteins can affect axon guidance or outgrowth in some ways *in vivo*.

Nestin-containing intermediate filaments are indeed well localized to influence growth cone behavior. Our own work shows striking accumulation of nestin in young cortical neurons, especially in the distal axon shaft and even in some peripheral regions of the axonal growth cone (Fig. 2). Nestin co-localizes with a subset of DCX, but is not identically distributed. This raises interesting future questions about why nestin is not transported into dendrites, and if this distribution is related to known differences in behavior of axonal and dendritic growth cones (i.e. differential guidance cue sensitivity)(X. Wang, Sterne, & Ye, 2014). Our findings suggest that nestin's distribution may contribute to spatial regulation of DCX phosphorylation and thus GC stability: nestin is absent from dendrites, which are known to have an opposite reaction to Sema3a (i.e. attractive) then axons (i.e. repulsive) (Polleux, Morrow, & Ghosh, 2000).

Summary

This work highlights how the intermediate filament composition of neurons can alter intracellular signaling pathways and thus alter the cells' morphology. Intermediate filaments have long been implicated as mediators and regulators of "cytoskeletal crosstalk" (Chang & Goldman, 2004; Michalczyk & Ziman, 2005), and our findings here represent an example of cytoskeletal crosstalk between IFs and MTs and their associated proteins. Our previous work has found that nestin expression correlated with small GC size and greater responsiveness to Sema3a. Conversely, depletion of nestin increased GC size and decreased Sema3a responsiveness, but it was not absolutely required for axon growth or response to Sema3a. Based on our new work, we implicate modulation of DCX phosphorylation by cdk5 as a relevant molecular pathway for neuronal nestin function. We thus posit that nestin sensitizes growth cones to cdk5 activity by scaffolding DCX, such that nestin-positive growth cones have higher levels of phosphorylated DCX at a given level of upstream cdk5 activation, compared to nestin-negative growth cones. Based on our data, we propose the model that nestin affects growth cone morphology as a kinase regulator. In addition to this signaling role, nestin could also play a structural role as a cytoskeletal filament, but more work will be required to more fully elucidate nestin's role in neurons. It will be of great interest to investigate how IFs might impact axon guidance during development.

Materials and Methods

293 Cell culture and transfection.

HEK293 cells were maintained in DMEM+10% fetal bovine serum, and all transfections were conducted using Lipofectamine 2000 (Invitrogen) according to the manufacturer's protocol. Phosphorylation assays and IPs were performed on low passage HEK 293s in 6cm plates. Cells in low serum (4%) were transfected for 24-26hrs, and serum starved for 10-14 hours prior to lysis, to reduce background activity of mitotic kinases. Total transfection time 34 to 40 hours.

Cos-7 cell culture and transfection.

Cos-7 cells were maintained in DMEM + 10% fetal bovine serum and all transfections were conducted using Lipofectamine 2000 (Invitrogen) according to the manufacturer's protocol. Cells were plated on , ethanol soaked, washed, round glass cell gro Fisherbrand coverslip in each 12 well plate well, at a density of 40k per well/coverslip. 2µg total of plasmid was used per transfection, and were carried out with equivalent amounts of GFP or GFP tagged construct, and empty vector myc or myc-tagged construct. The empty vector myc control is for a c-terminal myc tagged protein, thus has no start codon and is not expected to make any myc protein. Cells in low serum (4%) were transfected for 24-26hrs, and serum starved for 10-14 hours prior to lysis, to reduce background activity of mitotic kinases. Total transfection time was 34 to 40 hours.

Western Blot

Cells were washed with ice cold PBS, and lysed directly on the plate (6cm) into lysis buffer (500 µl); 50mM Tris HCl, 150mM NaCl, 1% NP-40, 1mM EDTA, 1mM DTT, 1mM PMSF, 1X HALT protease/phosphatase inhibitor cocktail. Extra NaF and NaOV was added in the lysis buffer for phosphorylation experiments in addition to that already in the cocktail. After incubating lysates on a rotisserie at 4° C for 30 minutes, lysate were cleared by centrifugation at 21K X g for 15 min at 4° C. We note that SPN is not well solubilized under these lysis condition, and we find that most of the SPN protein is in the pelleted material (not shown). Supernatants were diluted to 1x with 5X Laemmli buffer for western blot. Neuron cultures for Sema3a treatments where lysed directly in the 12 well plate well into 80-100ul 1.5x laemelli sample buffer for western blot. Samples were vortexed, boiled, and spun at 18k x g for 10 minutes prior to loading. For neurons, the protein equivalent to 100-150k neurons was loaded per lane. Equivalent amounts of cells within each experiment were run on a 4-20% polyacrylamide gel. After transfer onto nitrocellulose with the BioRad Transblot Turbo, membrane was blocked with Licor TBS blocking buffer for 1 hour at room temp. Primary and secondary antibodies were

diluted in 50% blocking buffer, 50% TBS, final 0.1% Tween-20. Primary antibodies were incubated overnight at 4° C, and after washing, followed by near-infrared secondary antibodies for 1 hour at room temperature. Blots were imaged with the dual color Licor Odyssey CLx imager, so each phospho-probe could be directly compared to the total protein in the same band. Densitometry of western blots was performed with Licor Image Studio software, the same software used to acquire the fluorescent blot images. The phospho antibody signal was divided by the total protein level (GFP tag or non-phospho specific antibody), and normalized to control. Positions of molecular weight ladders (in KD) are indicated next to the blot when there was room, otherwise the value of the approximate position in KD is shown.

Immunoprecipitation

Cell lysates were prepared as though for western blotting- 500ul of lysis buffer per 6cm dish of confluent cells. After the 21k x g spin, cells were precleared with 50µl of Thermo fisher control agarose for 4-6 hours. All incubations and washes were performed on the rotisserie at 4°C. For IP's for myc-tagged proteins, 12µl Bethyl goat anti-myc pre-conjugated beads were added to the pre-cleared lysate overnight. For IP's for other proteins (nestin, dcx, p35), 2µg of the relevant antibody was added to the precleared lysate for 4-6 hours, followed by addition of 12µl A/G beads overnight. Experiments using protein A/G beads for IP also used them for pre-clearing instead of the control agarose. After overnight incubation, IPs were washed 6 times in 500µl IP buffer. For GFP nano-body precipitations for phosphorylation assays, in order to minimize time and thus loss of phospho-epitopes, no pre-clearing was performed, the GFP-trap beads were immediately added to post-21K x g spin lysates for 1hr, and washed 2x. All IPs were eluted by addition of 2x sample buffer and immediate western blotting.

Neuronal Culture

Primary cultures of cortical neurons were obtained from embryonic day 16 (E16) mouse cortex of either sex as described in Bott et al., 2019. The protocol follows institutional ACUC protocols (approved animal protocol University of Virginia #3422). Cells were plated on acid-washed poly-L-lysine coated coverslips and incubated with Neurobasal medium with 10% fetal bovine serum and Penn/Strep. After 8 hrs, the cells were transferred into serum and antibiotic-free neurobasal medium supplemented with B27 (Invitrogen) and glutamax and cultured for a total of the indicated time periods *in vitro* (DIV). When WT vs DCX null neurons were compared within an experiment, mice were dissected and cultures prepared at the same time for consistency of comparison. For imaging purposes, cells were plated at ~100,000 cells per 15mm coverslip or at 130,000/coverslip in electroporation experiments. Cortical neurons for culture were harvested at E16, just prior to gliogenesis. Thus non-neuronal glia are rare in these cultures, but occasional nestin/Sox2 positive, GFAP negative persisting neural stem

cells were found. Cells were fixed at 24 hours (for non-transfection experiments) or 42-48 hours for overexpression experiments.
For co-IP experiments in neurons, cells were prepared similarly as described above. Six million untransfected cells were plated per 6 cm dish. At 24hours, the cells in the 6cm dish were lysed and subjected to DCX immunoprecipitation as described above.
Cells for Sema3a treatments and western blot, cells were prepared similarly as described above. Untransfected cells were plated at a density of 1 million cells per 12 well plate well. After 24 hrs, cells were treated with mouse Sema3a (R&D systems) diluted in growth media for 5, 15, or 30 minutes at 1nM as indicated. All conditions were subjected to 25nM calyculinA treatment 3 minutes prior to lysis to inhibit relevant phosphatase activity prior to lysis. After treatments, media was removed thoroughly and cells were quickly lysed directly into 1.5x laemmli sample buffer and subjected to western blotting as described above. In some experiments as indicated, cells were pre-treated with 10μM Roscovitine (Cayman Chemical) for 30 minutes prior to Sema3a treatment.

Neuron nucleofection
After cells were dissociated from E16 mouse cortex, cells were electroporated by Amaxa 4d nucleofection, according to manufacturer's protocols. 800,000 cells were electroporated in the small volume (20μl) cuvettes using P3 primary cell solution and CL-133 program. 0.1μg of GFP plasmid (pCMV-GFP-Clonetech) as a transfection marker, and 0.15μg of relevant myc-tagged construct was used in each nucleofection condition. The cells were then all plated in a 6cm dish containing 6 poly-L-lysine coated coverslips.

Immunofluorescence
Cells were fixed in prewarmed 4% Paraformaldehyde-PHEM-Sucrose (PPS: 60mM PIPES, 25mM HEPES, 10mM EGTA, 2mM MgCl2 (PHEM), 0.12M sucrose, 4% paraformaldehyde pH 7.4) for preservation of the cytoskeleton and cellular morphology and fixed at room temp for 16 min. Thorough permeabilization was required for nestin/intermediate filament visualization in neurons. Coverslips were permeabilized with 0.25% Triton-X 200 in 1% BSA/PBS for 20 min and then blocked for 30 min in 10% BSA, 5% normal donkey serum (NDS) in PBS all at room temperature. Primary antibodies were diluted in 1% BSA in PBS, and secondary antibodies in 1%BSA, 0.5% normal donkey serum in PBS. Primary antibody were incubated overnight at 4° C, and secondary antibodies for 90 min at room temperature. Appropriate species specific Alexa-350, -488, -568, or -647 labeled secondary antibodies raised in Donkey (Invitrogen and Jackson Immuno Research) were used for fluorescent labeling. Phalloidin-568 (Invitrogen) at 1:150 was used to visualize F-actin. Coverslips were mounted with ProLong Gold (Invitrogen). Widefield images for quantification were captured with a Zeiss Z1-Observer with a 40x objective. Images were captured with the Axiocam503 camera using Zen software (Zeiss) and processed identically within experiments. Confocal images of the whole neurons were captured with inverted Zeiss

LSM880 confocal microscope using a 63X objective. Enhanced resolution images of growth cones were captured using a Nikon TiE with A1 confocal microscope with a 100x objective and NA 1.49. Images were deconvolved using Landweber for 10 iterations. No non-linear image adjustments were performed.

In utero electroporation with CRISPR

The IUE CRISPR/Cas9 strategy is as follows: A gRNA sequence targeting the c-terminus of the Actb coding sequence (5'- AGTCCGCCTAGAAGCACTTG) was cloned into eSpCas9Opt1.1, expressing enhanced-specificity Cas9 and utilizing an optimized gRNA scaffold. To construct Actb_3xHA, tandem HA tag sequences were cloned between two Actb gRNA recognition sequences in the same orientation. Timed-pregnant dams were anesthetized with Ketamine (100 mg/kg) and Xylazine (10 mg/kg) via intraperitoneal injection, and given carprofen (5 mg/kg) via subcutaneous injection for analgesia. Uterine horns of an E13.5 pregnant CD-1 dam were exposed by midline incision. Lateral ventricles of embryos were injected with plasmid mix, composed of eSpCas9opt1.1-Actb_gRNA (1 µg/µl), Actb_3xHA (1.5 µg/µl), and CAG-Lifeact3xBFP (1 µg/µl), and 0.1% Fast Green FCF to visualize solution during intraventricular injection. *Successful genome editing and repair in a subset of transfected cells yielded an HA-tagged Actb locus and led to sparse expression of ACTB-3xHA in individual cells.* Electroporation paddles were positioned on opposing sides of the ventricle and 4 - 5 pulses of 27 volts (45 milliseconds each) were delivered, with 950 milliseconds between pulses, delivered using a BTX Harvard Apparatus ECM 830 power supply. Brains were isolated 3 days after electroporation, at E16.5, and fixed overnight in 4% PFA. These experiments were carried out in compliance with ethical regulations for animal research. The study protocol was reviewed and approved by the University of Michigan Institutional Animal Care & Use Committee.

Histology

Fixed in utero electroporated E16.5 mouse brains were then washed with PBS, embedded in agarose and vibratome sectioned into 100 um sections. Sections were stained as floating sections- permeabilized and blocked with 3% normal donkey serum + 0.3% Triton-X 100 in PBS for 1 hour at room temperature. Antibodies were diluted in the same permeabilization buffer with indicated primary and secondary antibodies sequentially overnight at 4°C. Sections were thoroughly washed over a period of 10hrs at room temperature with 0.5% BSA and 0.1% Triton-X 100 in PBS after primary and secondary antibody incubations. Sections were mounted on slides with Prolong Gold using 22X22mm 1.5 fisher brand coverslips. Confocal and Airyscan imaging of cryosections was carried out on an inverted Zeiss LSM880 confocal microscope (available in the UVA microscopy core facility) using a 63X objective.

Molecular biology

<u>Plasmids</u>

GFP-DCX (Yap et al., 2016)
Negative control substrates-GFP tagged:
    DCLK1 (Shin et al., 2013)
    Drebrin (addgene)
    FAK (addgene)
    Tau-YFP (George Bloom)
P35 (addgene)
HA-CDK5 (addgene)
HA-CDK5-DN (D145N) (addgene)
Myc-SPN Lawrence Brass (UPenn)(Yap et al., 2016)
INA-myc (Sino biological)
Nestin-myc (Bott2019 via original cDNA Bruce Lahn) PCR was used to generate EcoR1 and HindII sites on the 5' or 3" end respectively of full length mouse nestin. Both the insert and vector were treated with EcoR1 and HindII, the cut insert was ligated into pCDNA3.1 Myc-His(+) B.
Myc EV 3.1 B (stratagene)
GFP (Clonetech)
CMV-HA EV- (addgene)

New constructs made for this study:
Nestin mutants:
Nestin-myc T316A- We used to traditional primer mutagenesis for this plasmid derived from the pcDNA 3.1 B Nestin(wt)-myc plasmid. Only one nucleotide change was needed to mutate T(946ACA) to A(946GCA). Primer: 5'-gaacttcttccaggtgcctgcaagcgagagttc-3'
Nestin-myc T316D- Could not be obtained via traditional mutagenesis and was made, instead via gene synthesis from genscript of a large >1kb piece of nestin that included the three nucleotide changes- T(946ACA) to D(946GAT). The 5' end had a HINDIII site for incorporation into the MCS of pcDNA 3.1 B nestin(wt)-myc plasmid. An ECOR1 site present in WT nestin was used for the 3" end.

Image analysis
All image analysis was performed on ImageJ blinded to experimental conditions. Transfected cells were identified by having a prominent GFP fluorescence. Stage3 neurons were identified (according to Banker staging) by having one neurite (the future axon) at least 2x longer than the next longest neurite. The distal portion of the future axon was analyzed for morphological measurements as the "axon growth cone". Images were analyzed as in Bott et al. 2019.
Filopodial protrusions were counted using the phalloidin channel, and any protrusions from the growth cone were counted.
Axon length was the length of the axon from the cell body to the growth cone tip as in Bott et al. 2019.

Growth cone area were assessed by measuring traced outlines the growth cone not counting the filopodial protrusions, and extending down proximally to the point where the splayed growth cone microtubules consolidate into bundles in axon shaft as in Bott et al. 2019.

Statistical analysis

All data was statistically analyzed using Prism software. Datasets were first evaluated for normality by using the Shapiro-Wilk normality test. This result was used to decide if parametric or non-parametric tests were to be used. When more than one comparison was made, the corresponding ANOVA test was used. When only two conditions were compared, we used a t-test. Figure legends specify details- for each set of experiments we made an effort to show precise p-values when shown. p-values reaching statistical significance of at least <0.05 are in **bold**.

Microscope image acquisition

Widefield images for quantification were captured with a Zeiss Z1-Observer with a 40x objective. Images were captured with the Axiocam503 camera using Zen software (Zeiss) and processed identically within experiments.
Confocal images of the whole neurons or brain sections were captured with inverted Zeiss LSM880 confocal microscope using a 63X objective with Zen software. Airyscan was used for some brain section imaging.
Enhanced resolution images of growth cones were captured using a Nikon TiE with A1 confocal microscope with a 100x objective and NA 1.49. Images were deconvolved using Landweber for 10 iterations. No non-linear image adjustments were performed.

Reagents

Antibodies

Mouse anti-Nestin 2Q178 1:200 IF, 1:500 IHC, 1:500 WB **Santa Cruz Biotechnology Cat# sc-58813 RRID:AB_784786**
Goat anti-Nestin R-20: Raised against peptide in the unique C-terminal tail region of nestin 1:200 IHC **Santa Cruz Biotechnology Cat# sc-21249 RRID:AB_2267112**
Rabbit anti-DCX- 1:1200 IF, IHC, 1:4000 WB **Abcam Cat# ab18723 RRID:AB_732011**
Mouse anti- βIII Tubulin Tuj1- 1:800 IF A generous gift from the Deppman Lab YVA **A. Frankfurter, University of Virginia; Department of Biology Cat# TuJ1 (beta III tubulin) RRID:AB_2315517**
Chicken anti-βIII tubulin- 1:200 IF **Aves Labs Cat# TUJ RRID:AB_2313564**
Rat anti α-tubulin- 1:2000 WB **Santa Cruz Biotechnology Cat# sc-53030 RRID:AB_2272440**

Rabbit anti-Vimentin- 1:100 IF, 1:100 IHC, 1:1000 WB **Bioss Inc Cat# bs-0756R RRID:AB_10855343**
Rabbit anti-Vimentin 1:1000 IF **Abcam Cat# ab92547, RRID:AB_10562134**
Mouse anti-Myc tag 9E10: 1:1000 WB, 1:200 IF **Santa Cruz Biotechnology Cat# sc-40, RRID:AB_627268**
Rat anti-Myc tag 9E1- 1:1000 WB ChromoTek Cat# 9e1-100, RRID:AB_2631398
Rat anti-HA 1:2000 WB **ChromoTek Cat# 7c9, RRID:AB_2631399**
Rabbit anti-GFP D5.1 1:5000 WB **Cell Signaling Technology Cat# 2956, RRID:AB_1196615**
Mouse anti-GFP N86/8 1:5000 WB **UC Davis/NIH NeuroMab Facility Cat# 73-131, RRID:AB_10671444**
Rabbit anti-CDK substrate multiMab 1:1000 WB **Cell Signaling Technology Cat# 9477, RRID:AB_2714143**
Rabbit anti-pS297 DCX 1:1000 WB **Cell Signaling Technology Cat# 4605, RRID:AB_823682**
Rabbit anti-pS334 DCX 1:2000 WB **Cell Signaling Technology Cat# 3453, RRID:AB_2088485**
Mouse anti-CDK5 1:2000 WB **1H3 Cell Signaling Technology Cat# 12134, RRID:AB_2797826**
Rabbit anti-p35/p25 1:2000 WB **C64B10 Cell Signaling Technology Cat# 2680, RRID:AB_1078214**
Mouse anti-Spinophilin (Neurabin II) 1:2000 WB **Santa Cruz Biotechnology Cat# sc-373974, RRID:AB_10918794**
Mouse anti-Drebrin 1:2000 WB **Santa Cruz Biotechnology Cat# sc-374269, RRID:AB_10990108**
Mouse anti- Phf1 tau- supernatant 1:50 WB **P. Davies Albert Einstein College of Medicine; New York; USA Cat# PHF1, RRID:AB_2315150. A gift from George Bloom.**
Rabbit anti-pS522 Crmp2a 1:1000 WB **Thermo Fisher Scientific Cat# PA5-37550, RRID:AB_255415**
Mouse anti-pS732 FAK 1:1000 WB **Santa Cruz Biotechnology Cat# sc-81493, RRID:AB_1125825**
Rabbit anti-pY397 FAK 1:1000 WB **Bioss Cat# bs-1642R, RRID:AB_10856939**
Gt anti-myc agarose 1:50 IP **Bethyl Cat# S190-104, RRID:AB_66618**
GFP trap agarose 1:100 IP **ChromoTek Cat# gta-20, RRID:AB_2631357**
GFP booster nanobody- 1:600 IF **ChromoTek Cat# gba488-100 RRID:AB_2631434**
Phalloidin 568 1:150 Invitrogen

Cell lines
Hek293 cell lines: **ATCC Cat# PTA-4488, RRID:CVCL_0045**
Cos7 cell lines: **ATCC Cat# CRL-1651, RRID:CVCL_0224**

Supplemental Material Summary

Fig S1 shows how nestin and DCX co-localize when overexpressed in COS7 cells. Fig S2 describes out in utero electroporation strategy, and include an example of a nestin negative neuron. Fig S3 shows a repeat of the DCX phosphorylation assay, but with an additional antibody- replicating the results in Fig 3. In addition, the relevance of the pS297 epitope in 1DIV cortical neurons is shown by increasing levels of this epitope by western blot after a Sema3a time course. Fig S4 show that the nestin mutants associate with vimentin similarly. In addition, the T316D mutant does not associate with DCX, unlike WT or T316D nestin.

Figure Legends

Figure1: Nestin specifically interacts with the cdk5 substrate doublecortin.

A. Candidate screen for cdk5 substrates that interact with nestin by co-immunoprecipitation (co-IP). Six different GFP-tagged cdk5 substrates were expressed with or without nestin-myc in HEK293 cells and subjected to immunoprecipitation with anti-myc antibody. An empty vector was used as a negative control. Top panel: Input lysates are shown. αTubulin is used as a loading control. Bottom panel: Anti-myc IPs are probed against myc or GFP. Only GFP-DCX co-IPs with nestin-myc. A'. Densitometry analysis of each co-IP'ed substrate relative to its input. Statistical comparisons (ordinary one-way ANOVA with Sidak's correction) were performed between the empty vector myc IP compared to nestin-myc IP. Errors bars are SD, n = at least 3 for each condition. P-values are indicated above the graph.

B - B'. IP of endogenous nestin and DCX complexes from brain. B. DCX co-IP with nestin antibody from E17 rat brain compared to a control IgG. B'. Nestin co-IP with DCX antibody from E17 rat brain compared to a control IgG. As a positive control, DCX IPs were probed against SPN. Drebrin, serves as a negative control.

C. anti-DCX immunoprecipitation from 1DIV cortical E16 mouse neurons results in co-IP of nestin from WT neurons, but not DCX knockout (null) neurons, demonstrating specificity of the IP. No anti-DCX immunoreactivity is seen in the western blots of DCX null neurons compared to WT, also demonstrating specificity of the antibody.

Figure 2: Nestin co-localizes with DCX in axons of newly born neurons in vitro and in vivo.

A. Confocal images of an E16 cortical mouse stage 3 neuron after 1 DIV culture, counterstained for DCX, nestin, and β3 tubulin. DCX is enriched at the distal region of

all neurites, whereas nestin immunostaining labels only the distal region of the growing axon (arrowhead), but not of the minor neurites.

B. Enhanced resolution confocal imaging of nestin in the distal region of an axon- together with DCX MT bundle. Distally, some nestin filaments appear to extend into the central region of the growth cone and into some proximal filopodia.

C. Wide field immunofluorescence image of a coronal section of E16.5 mouse cortex to illustrate the sparse labeling of individual neurons achieved with knockin of HA-tag using CRISPR and IUE. In all panels, red arrowhead indicates the cell body that projects the HA/Nes/DCX positive growth cone. * marks the nestin positive growth cone, whereas # marks the nestin negative neuron (shown in Fig. S2B). The major cortical layers are labeled: VZ- ventricular zone, IZ- intermediate zone, CP- cortical plate. Antibody labeling is indicated in each panel. C', C'', and C''' panels are confocal images, and C'''' is an airyscan enhanced resolution image. C'. Inset of square in C demonstrating HA-staining of a single stage 3 neuron with the entirety of its axon imaged in a confocal stack (maximum projection). C''. High magnification zoom of the inset square of C' marked with * in C and C'. A single z-plane of each channel shown. C'''. Orthogonal projection of the region indicated in the red dashed line of C''. The red box outlines the relevant HA-labeled cell. C''''. High magnification Zeiss Airyscan confocal image equivalent of C''.

Figure 3: <u>Nestin specifically increases cdk5-dependent phosphorylation of DCX</u>

A. Myc Empty Vector (EV), Nestin-myc, INA-myc (negative control), or myc-SPN were expressed in HEK293 cells with DCX alone (-), or with both p35 and DCX (+). Cell lysates were run on two replicate western blots and both blotted against GFP for total levels of GFP-DCX. Each was blotted with the relevant phospho-specific antibodies to pS297-DCX (a cdk5 site) or pS334-DCX (a JNK site). The levels/presence of relevant proteins are shown, including ckd5 (endogenous), p35 (overexpressed), tubulin (endogenous, loading control), and the overexpressed myc-tagged constructs. Arrows point at the relevant myc-tagged protein bands. A'. Quantification of A by densitometry. Ratio of phospho-DCX to total DCX are plotted. Black bars represent pS297-DCX/total DCX, and red bars represent pS334-DCX/total DCX- colors correspond to the outline around the relevant blot. Error bars are SD. N = 4 to 6 independent experiments. Every condition was compared to every other condition with an ordinary one way ANOVA test with Tukey correction. P-values compared pairwise to control (CON) are shown. Additional comparisons not shown are pS297 level in Nestin + p35 condition is significantly different than p35 alone ($p<0.0001$) and nestin alone ($p=0.0004$), while pS334 is not significantly different (>0.9999 and 0.8979 respectively) for the same comparisons.

B. HEK293 cells transfected simultaneously with p35, nestin-myc, and GFP-DCX were treated with inhibitors of cdk5 (roscovitine), JNK (SP600125), cdk1 (Ro2206), or vehicle (UNT) for 6h before lysis. Only roscovitine significantly decreased levels of pS297-DCX. B'. Quantification of the blots in B. Error bars shown are SD, ordinary one-way ANOVA with Dunnett's correction was performed and the pairwaise p-values are shown for each condition compared to untreated control (UNT). N=3-5 independent experiments.

Figure 4: DCX requires nestin with cdk5/p35 for significant phosphorylation, unlike other cdk5 substrates which only require cdk5/p35.

A-F. Comparison of levels of phosphorylation of several cdk5 substrates with the indicated transfection conditions: Myc EV – left lane, Myc + p35 – middle lane, Nes-myc + p35 – right lane. Cdk5-dependent phospho-sites on Crmp2a (A), tau (B), FAK (C) and DCX (E) were assessed for p35- and nestin-dependence. The pY397 site on FAK (D) is a negative control because cdk5 is a Ser/Thr kinase. pS334 on DCX is a JNK site (F) and serves as a negative control. The values for DCX phosphorylation are from additional independent experiments separate from those in 3A'.

A'-F'. The level of phosphorylation of each substrate was quantified by densitometry analysis of the phospho-signal compared to total (GFP) and graphed to the right of each blot. Error bars are SD. The statistical test used was one-way ANOVA with Tukey's correction. N= 3 or 4 independent experiments.

G. Variable amounts of p35 plasmid (0, 1, 2, 4 µg) were transfected to increase levels of p35 expression in the absence of nestin. In addition, nestin was co-expressed with 0 or 1 µg p35 plasmid (+Nes lanes). GFP-DCX was expressed in every condition. Levels of pS297-DCX and pS334-DCX were determined by Western blotting. Levels of GFP-DCX, p35, cdk5 are also assayed. A longer exposure of the p35 blot is shown to illustrate negligible levels of the proteolytic product p25 form of p35. G'. Densitometry analysis of G. Black bars are ratio of pS297-DCX/total GFP-DCX, red bars are ratio of pS334-DCX/total GFP-DCX. Error bars are SD. Statistical analysis was one way ANOVA with Dunnet's correction. Significant pairwise p-values compared to control (Con) are indicated in black for pS297 and in red for pS334. All other pairwise comparisons to control were not significant and are not shown. N=4 independent experiments.

Figure 5: Nestin scaffolds cdk5 and DCX to promote DCX phosphorylation.

A. Experimental design model for using the kinase dead (KD) cdk5- D145N: Kinase-dead cdk5 forms a quaternary complex with p35, nestin and DCX which is stable. WT cdk5 more transiently associates with its substrate DCX and does not form a stable complex (which is a typical relationship between the kinase and substrate).

B. KD cdk5 increases efficiency of nestin pulldowns for DCX. GFP-DCX and p35 was co-transfected with myc EV, nes-myc, or INA-myc together with HA-cdk5-WT or HA-

cdk5-KD, as indicated above the lanes, and IPed with anti-myc antibody. GFP-DCX inputs (top blot) were compared to amounts of immunoprecipitated GFP-DCX after anti-myc IPs (bottom two blots). B'. The amount of DCX after nestin IP is shown as a ratio of the co-IP to input DCX. HA-cdk5-KD was compared to HA-cdk5-WT after nestin IP. This ratio was set to 1 for cdk5-KD. With cdk5-KD, DCX is trapped in a stable complex with nestin. Error bars are SD, and statistics were unpaired t-test. N= 6 independent experiments.

C. P35 co-IPs more DCX when nestin is co-expressed. Transfection conditions are indicated above each lane. HA-cdk5-KD is expressed in each condition to stabilize the kinase/substrate/scaffold complex. Input levels in the lysate (left panel) are compared to levels of GFP-DCX IPed with anti-p35 antibody (right panel). Nestin increases the amount of DCX that co-IP's with p35. C'. Relative densitometry analysis of DCX in p35 co-IP compared to DCX in input. Error bars are SD, and statistical analysis was t-test with welches correction. N= 3 independent experiments.

D. Model for how nestin increases cdk5-phosphorylation of DCX by scaffolding: in the absence of nestin (-Nestin; top) non-phospho-DCX is bound to microtubules and inefficiently phosphorylated by cdk5/p35. In the presence of nestin (+ Nestin scaffold; bottom), DCX becomes associated with cdk5/p35, increasing the efficiency of phosphorylation. We include in the model data from others that showed that the actin-associated SPN with Protein Phosphatase 1 (PP1) can dephosphorylate DCX. In our model, the level of phospho-DCX is determined by the relative opposing activities of the two regulatory complexes.

Figure 6: <u>A DCX and p35-binding deficient nestin mutant no longer affects growth cone size of DIV2 cortical neurons.</u>

A. Point mutants in nestin (T316A - phospho dead or T316D - putative phospho mimetic) were tested for binding to p35, DCX, and vimentin by co-IP from HEK293 cells. Inputs (left blot) and corresponding co-immunoprecipitation of Vimentin, GFP-DCX, and p35 after anti-myc IP (right blot) are shown. T316D-nestin has greatly reduced levels of co-IP of p35 and DCX compared to WT nestin and T316A-nestin. Each mutant co-IPs vimentin similarly. [Note, the p35 and DCX/vimentin panels are combined from the same experiment expressed in two different set of cells. The blots are qualitatively similar for both sets of cells, and were combined into a single figure for simpler viewing.]

B. Nestin-dependent cdk5-phosphorylation of DCX in HEK293 cells. B'. Densitometry quantification of the blot in B showing the relative levels of pS297-DCX phosphorylation with expression of each mutant. Each value represents the relative phosphorylation of DCX when expressed with nestin and p35, compared to just nestin expression. T316D-nestin does not augment p35/CDK5-mediated DCX phosphorylation. Error bars are SD, and each condition was compared to WT nestin condition (one way ANOVA with Dunnett's correction). N= 3 independent experiments.

C. Representative images of DIV2 cortical neurons expressing nestin or T316-nestin mutants compared to empty vector control or INA-myc. β3 tubulin and phalloidin were used to visualize MTs and F-actin, respectively. Axonal GCs are indicated with arrows, and secondary neurites (dendrites), are labeled with arrowheads. Brightness was adjusted for each image for easier viewing. Insets show transfected neurons, identified by GFP expression.

C', C'', and C'''. Quantification of neuronal morphology in neurons expressing different nestin constructs (as shown in C). N= 72 to 61 cells counted per condition in 3 different independent experiments. Data was analyzed with non-parametric Kruskal-Wallis test with Dunn's correction. Pairwise p-values are shown for comparisons to myc EV (control). WT nestin and T316A-nestin decrease growth cone area and filopodia number, but T316D-nestin does not.

Figure 7: In the absence of DCX, nestin does not cause small growth cones.

A. Representative images of WT or DCX null E16 neurons (as labeled) expressing nes-myc with GFP or nes-myc with GFP-DCX after 48 hours in culture. WT neurons transfected with nes-myc show smaller axonal GCs (arrows) whereas DCX KO neurons transfected with nestin-myc do not show smaller GCs. When GFP-DCX is co-transfected into DCX KO neurons, small GCs are rescued. Axon growth cones are indicated with arrows. The growth cones of secondary neurites (dendrites) where not considered and are indicated with arrowheads.

B',B", B"'. Quantification of morphological characteristics. The background shading color behind the images in A correspond to the conditions shaded in the graphs B', B'', and B''' for easier interpretation. B', B'', and B''' shows the quantification of morphological measurements from transfected neurons: growth cone area (B'), filopodia number (B"), and axon length (B"'). Error bars are SD. Kruskal-Wallis non-parametric test was used. P-values are only shown for selected statistical comparisons to keep the graph less cluttered. N= 40 to 70 cells counted in 3 different independent experiments.

Figure legends for Supplementary Figures

Supplement 1

Nestin co-localizes with DCX-MT bundles.

A-E: Confocal images of COS-7 cells transfected with GFP-DCX + myc EV (A), GFP + nes-myc (B), GFP-DCX + nes-myc (C), GFP-DCX+ INA-myc (D), and YFP-tau + nes-myc (E). All cells are counterstained with GFP booster nanobody, anti-myc tag antibody, and antibody against endogenous vimentin, as labeled above each panel column. Each cell is outlined with a dotted line. Individual black and white images are shown for each channel separately, as well as merged images of the GFP/myc and myc/vimentin Channels. Panel outlines of black and white images correspond to the

color used in the composite images. Nestin is associated with vimentin in the perinuclear region, except when GFP-DCX is co-expressed which recruits nestin onto DCX MT bundles. Vimentin remains in the perinuclear region. Tau and internexin are additional negative controls.

Supplement 2

A. Diagram of the experimental strategy to detect nestin and DCX in single growth cones in mouse cortex. E13.5 mouse cortex was electroporated *in utero* to sparsely introduce three HA-tags into β-actin (Actb-3xHA) by CRISPR. Brains were fixed at E16.5. The CRISPR strategy is depicted diagrammatically.

B. High magnification zoom of the growth cone marked with "#" in figure 2C. Arrowheads point along the length of the axon, nestin is not detected in this growth cone.

Supplement 3

A. Phosphorylation of GFP-DCX in HEK293 cells transfected similarly to Figure 3 using an antibody to a generic K/H SP cdk5 phosphorylation motif. Because many proteins in 293 cell lysate can be recognized with this antibody, cell lysates were subjected to GFP-trap incubation and precipitation to isolate GFP-tagged DCX from other reactive proteins and subsequently subjected to western blot. A'. Densitometry quantification of A where levels of signal to the phospho-reactive antibody is ratio-ed to the level of total DCX. Error bars are SD and a one way ANOVA with Dunnett's correction was used to compare each condition to the control cells transfected with the GFP-DCX substrate only. N= 3 independent experiments.

B. Sema3a treatment of 1DIV cultured mouse cortical E16 neurons increases DCX phosphorylation S297, but not at S334. Rightmost lane: Neurons were treated with 1nM Sema3a for 5 min with pre-incubation of the cells with 10μM Roscovitine for 30 minutes. The inhibitor lane was from the same blot as the other lanes, but separated by intervening lanes which were removed. B'. Quantification of Sema3a time course. Blots in B were subjected to densitometry analysis, and the ratio of phospho-DCX signal relative to the total DCX is plotted. DCX phosphorylation at pS297, but not at pS334, begins quickly after Sema3a stimulation, and becomes significant at 15 and 30 minutes. Error bars are SD and statistical analysis was performed at each timepoint compared to untreated (UNT) with an ordinary one way Anova with Dunnett's correction. n=5 independent experiments. B''. Quantification of Roscovitine sensitivity (rightmost lane in B). Each value was obtained from densitometry analysis of western blots, where the relative level of p-DCX was compared to total DCX. The values in the plot are a ratio of the relative phosphorylation after inhibitor (drug) treatment compared to no inhibitor

treatment. Error bars are SD and statistical analysis was performed with a two-tailed unpaired t-test. N=5 independent experiments.

Supplement 4

Confocal images of COS-7 cells transfected with GFP (A-C) or GFP-DCX (D-F) co-transfected with WT nes-myc (A,D) or mutant nestin (T316A: B, E. T316D: C, F), as indicated. Each cell is outlined with a dotted line. Individual black and white channels are shown, as well as merges with GFP/myc and myc/vimentin channels. Outlines of black and white images correspond to the color used in the composite images. WT nestin and the 316A-nestin mutant associate with DCX MT bundles. However, nestin is associated with vimentin when expressed without DCX or when the DCX-binding deficient T316D-nestin is expressed, even in the presence of DCX.

References

Bahi-Buisson, N., Souville, I., Fourniol, F. J., Toussaint, A., Moores, C. a, Houdusse, A., … Francis, F. (2013). New insights into genotype-phenotype correlations for the doublecortin-related lissencephaly spectrum. *Brain : A Journal of Neurology*, *136*(Pt 1), 223–244.

Benson, D. L., Mandell J. W., Shaw G., B. G. (1996). Compartmentation of alpha-internexin and neurofilament triplet proteins in cultured hippocampal neurons. *Journal of Neurocytology*, *25*(3), 181–196.

Bielas, S. L., Serneo, F. F., Chechlacz, M., Deerinck, T. J., Perkins, G. a., Allen, P. B., … Gleeson, J. G. (2007). Spinophilin Facilitates Dephosphorylation of Doublecortin by PP1 to Mediate Microtubule Bundling at the Axonal Wrist. *Cell*, *129*(3), 579–591.

Bott, C. J., Johnson, C. G., Yap, C. C., Dwyer, N. D., Litwa, K. A., & Winckler, B. (2019). Nestin in immature embryonic neurons affects axon growth cone morphology and Semaphorin3a sensitivity. *MBOC*, *30*(10), 1214–1229.

Bourgeois, F., Mess??ant, J., Kordeli, E., Petit, J. M., Delers, P., Bahi-Buisson, N., … Legay, C. (2015). A critical and previously unsuspected role for doublecortin at the neuromuscular junction in mouse and human. *Neuromuscular Disorders*, *25*(6), 461–473.

Boyne, L. J., Fischer, I., & Shea, T. B. (1996). Role of vimentin in early stages of neuritogenesis in cultured hippocampal neurons. *International Journal of Developmental Neuroscience*, *14*, 739–748.

Brown, A. (2013). Axonal Transport. In *Neuroscience in the 21st Century* (pp. 255–308).

C. Kappeler, M. Dhenain, F. Phan Dinh Tuy, Y. Saillour, S. Marty, C. Fallet-Bianco, I.

Souville, E. Souil, JM. Pinard, G. Meyer, F. Encha-Razavi, A. Volk, C. Beldjord, J. Chellly, F. F. (2007). Magnetic Resonance Imaging and Histological Studies of Corpus Callosal and Hippocampal Abnormalities Linked to doublecortin Deficienc. *The Journal of Comparative Neurology*, *500*(Jan 10), 239–254.

Chang, L., & Goldman, R. D. (2004). Intermediate filaments mediate cytoskeletal crosstalk. *Nature Reviews. Molecular Cell Biology*, *5*(8), 601–613.

Dent, E. W., & Gertler, F. B. (2003). Cytoskeletal dynamics and transport in growth cone motility and guidance. *Neuron*, *40*(2), 209–227.

Dent, E. W., Gupton, S. L., & Gertler, F. B. (2011). The growth cone cytoskeleton in axon outgrowth and guidance. *Cold Spring Harbor Perspectives in Biology*, *3*(3), 1–39.

Dubey, M., Hoda, S., Chan, W. K. H., Pimenta, A., Ortiz, D. D., & Shea, T. B. (2004). Reexpression of vimentin in differentiated neuroblastoma cells enhances elongation of axonal neurites. *Journal of Neuroscience Research*, *78*(2), 245–249.

E. Goldsmith, R. Akella, X. Min, T. Zhou, J. H. (2007). Substrate and Docking Interactions in Ser/Thr Protein Kinases Elizabeth. *Chemical Reviews*, *107*(11), 5065–5081.

Elder, G. A., Friedrich, V. L., Bosco, P., Kang, C., Gourov, A., Tu, P., … Lazzarini, R. A. (1998). Absence of the Mid-sized Neurofilament Subunit Decreases Axonal Calibers, Levels of Light Neurofilament (NF-L), and Neurofilament Content. *The Journal of Cell Biology*, *141*(3), 727–739.

Eva, R., & Fawcett, J. (2014). Integrin signalling and traffic during axon growth and regeneration. *Current Opinion in Neurobiology*, *27C*, 179–185.

Friocourt, G, Chafey, P., Billuart, P., Koulakoff, a, Vinet, M. C., Schaar, B. T., … Chelly, J. (2001). Doublecortin interacts with mu subunits of clathrin adaptor complexes in the developing nervous system. *Molecular and Cellular Neurosciences*, *18*, 307–319.

Friocourt, Gaëlle, Koulakoff, A., Chafey, P., Boucher, D., Fauchereau, F., Chelly, J., & Francis, F. (2003). Doublecortin functions at the extremities of growing neuronal processes. *Cerebral Cortex*, *13*, 620–626.

Fu, X., Brown, K. J., Yap, C. C., Winckler, B., Jaiswal, J. K., & Liu, J. S. (2013). Doublecortin (Dcx) Family Proteins Regulate Filamentous Actin Structure in Developing Neurons. *The Journal of Neuroscience*, *33*(2), 709–721.

Gdalyahu, A., Ghosh, I., Levy, T., Sapir, T., Sapoznik, S., Fishler, Y., … Reiner, O. (2004). DCX, a new mediator of the JNK pathway. *The EMBO Journal*, *23*(4), 823–832.

Ge, W., He, F., Kim, K. J., Blanchi, B., Coskun, V., Nguyen, L., … Sun, Y. E. (2006). Coupling of cell migration with neurogenesis by proneural bHLH factors. *Proceedings of the National Academy of Sciences of the United States of America*, *103*(5), 1319–1324.

Geraldo, S., & Gordon-Weeks, P. R. (2009). Cytoskeletal dynamics in growth-cone steering. *Journal of Cell Science*, *122*(Pt 20), 3595–3604.

Gleeson, J. G., Peter T, L., Flanagan, L. a., & Walsh, C. a. (1999). Doublecortin is a microtubule-associated protein and is expressed widely by migrating neurons. *Neuron*, *23*(2), 257–271.

Graham, M. E., Ruma-haynes, P., Capes-davis, A. G., Dunn, J. M., Tan, T. C., Valova, V. A., … Jeffrey, P. L. (2004). Multisite phosphorylation of doublecortin by cyclin-dependent kinase 5. *Biochem. J.*, *381*, 471–481.

Grant, N. J., Coates, P. J., Woods, Y. L., Bray, S. E., Morrice, N. A., Hastie, C. J., … Sutherland, C. (2015). Phosphorylation of a splice variant of collapsin response mediator protein 2 in the nucleus of tumour cells links cyclin dependent kinase-5 to oncogenesis. *BMC Cancer*, *15*, 1–16.

Gumy, L. F., Chew, D. J., Tortosa, E., Katrukha, E. A., Kapitein, L. C., Tolkovsky, A. M., … Fawcett, J. W. (2013). The Kinesin-2 Family Member KIF3C Regulates Microtubule Dynamics and Is Required for Axon Growth and Regeneration. *The Journal of Neuroscience*, *33*(28), 11329–11345.

Huang, Y., Wu, C., Shi, G., & Wu, G. C. (2017). Nestin Serves as a Prosurvival Determinant that is Linked to the Cytoprotective Effect of Epidermal Growth Factor in Rat Vascular Smooth Muscle Cells. *Journal of Biochemistry*, *146*(October), 307–315.

Jean, D. C., Baas, P. W., & Black, M. M. (2012). A novel role for doublecortin and doublecortin-like kinase in regulating growth cone microtubules. *Human Molecular Genetics*, *21*(26), 5511–5527.

K. Pennypacker, I. Fischer, P. L. (1991). Early in Vitro Genesis and Differentiation of Axons and Dendrites by Hippocampal Neurons Analyzed Quantitatively with Neurofilament-H and Microtubule-Associated Protein 2 Antibodies. *Experimental Neurology*, *111*(Jan), 25–35.

Kapitein, L. C., & Hoogenraad, C. C. (2015). Building the Neuronal Microtubule Cytoskeleton. *Neuron*, *87*(3), 492–506.

Kiss, A., Fischer, I., Kleele, T., Misgeld, T., & Propst, F. (2018). Neuronal Growth Cone Size-Dependent and -Independent Parameters of Microtubule Polymerization. *Frontiers in Cellular Neuroscience*, *12*(July), 1–15.

Kreis, P., Gallrein, C., Rojas-Puente, E., Mack, T. G., Kroon, C., Dinkel, V., … Eickholt, B. J. (2019). ATM phosphorylation of the actin-binding protein drebrin controls oxidation stress-resistance in mammalian neurons and C. elegans. *Nature Communications*, *486*(10), 1–13.

L. Dehmelt, S. H. (2007). Neurite outgrowth. A Flick of the wrist. *Current Biology*, *17*(15), 609–611.

Lariviere, R. C., & Julien, J. (2003). Functions of Intermediate Filaments in Neuronal Development and Disease. *Journal of Neurobiology*, *58*(1), 131–148.

Laser-Azogui, A., Kornreich, M., Malka-Gibor, E., & Beck, R. (2015). Neurofilament assembly and function during neuronal development. *Current Opinion in Cell Biology*, *32*(2), 92–101.

Lee, S., & Shea, T. B. (2014). The high molecular weight neurofilament subunit plays an essential role in axonal outgrowth and stabilization. *Biology Open*, *3*(10), 974–981.

Lew, J., Huang, Q., Qi, Z., Winkfeln, R. J., Aebersold, R., Hunt, T., & Wang, J. H. (1994). A brain-specific activator of cyclin-dependent kinase 5. *Nature*, *371*(September), 423–426.

Lew, J., Winkfein, R. J., Paudel, H. K., & Wang, H. (1992). Brain Proline-directed Protein Kinase Is a Neurofilament Kinase Which Displays High Sequence Homology to p34cdc2. *Journal of Biological Chemistry*, *267*(36), 25922–25926.

Lin, W., Dominguez, B., Yang, J., Aryal, P., Brandon, E. P., Gage, F. H., & Lee, K. (2005). Neurotransmitter Acetylcholine Negatively Regulates Neuromuscular Synapse Formation by a Cdk5-Dependent Mechanism. *Neuron*, *46*(5), 569–579.

Lin, W., & Szaro, B. G. (1996). Effects of Intermediate Filament Disruption on the Early Development of the Peripheral Nervous System of Xenopus laevis. *Developmental Biology*, *211*(0251), 197–211.

Lindqvist, J., Torvaldson, E., Gullmets, J., Karvonen, H., Nagy, A., Taimen, P., & Eriksson, J. E. (2017). Nestin contributes to skeletal muscle homeostasis and regeneration. *Journal of Cell Science*, *130*, 2833–2842.

Manning, B. D., & Cantley, L. C. (2002). Hitting the Target : Emerging Technologies in the Search for Kinase Substrates. *Sci STKE*, *162*(12), 1–5.

Menon, S., & Gupton, S. L. (2016). Building Blocks of Functioning Brain : Cytoskeletal Dynamics in Neuronal Development. In *International Review of Cell and Molecular BiologyInternational Review of Cell and Molecular Biology* (Vol. 3, pp. 183–245). Elsevier Inc.

Meyerson, M., Enders, G. H., Wu, C., Su, L., Gorkal, C., Nelson, C., … Tsai, L. (1992). A family of human cdc2-related protein kinases. *EMBO Journal*, *11*(8), 2909–2917.

Michalczyk, K., & Ziman, M. (2005). Nestin structure and predicted function in cellular cytoskeletal organisation. *Histology and Histopathology*, *20*, 665–671.

Miller, K. E., & Suter, D. M. (2018). An Integrated Cytoskeletal Model of Neurite Outgrowth. *Frontiers in Cellular Neuroscience*, *12*(November), 1–19.

Mohseni, P., Sung, H.-K., Murphy, A. J., Laliberte, C. L., Pallari, H.-M., Henkelman, M., … Nagy, A. (2011). Nestin is not essential for development of the CNS but required for dispersion of acetylcholine receptor clusters at the area of neuromuscular junctions. *The Journal of Neuroscience : The Official Journal of the Society for Neuroscience*, *31*(32), 11547–11552.

Moores, C. A., Perderiset, M., Francis, F., Chelly, J., Houdusse, A., & Milligan, R. A. (2004). Mechanism of microtubule stabilization by doublecortin. *Molecular Cell*,

14(6), 833–839.

Moslehi, M., Ng, D. C. H., & Bogoyevitch, M. A. (2017). Dynamic microtubule association of Doublecortin X (DCX) is regulated by its C-terminus. *Scientific Reports*, *5245*(7), 1–11.

Namba, T., Kibe, Y., Funahashi, Y., Nakamuta, S., Takano, T., Ueno, T., … Takeuchi, K. (2014). Pioneering Axons Regulate Neuronal Polarization in the Developing Cerebral Cortex. *Neuron*, *81*(4), 814–829.

Ng, T., Ryu, J. R., Sohn, J. H., Tan, T., Song, H., Ming, G. L., & Goh, E. L. K. (2013). Class 3 Semaphorin Mediates Dendrite Growth in Adult Newborn Neurons through Cdk5/FAK Pathway. *PLoS ONE*, *8*(6), 1–15.

Nishimura, Y. V, Shikanai, M., Hoshino, M., Ohshima, T., & Nabeshima, Y. (2014). Cdk5 and its substrates, Dcx and p27 kip1, regulate cytoplasmic dilation formation and nuclear elongation in migrating neurons. *Development*, *141*(18), 3540–3550.

Nixon, R. A., & Shea, T. B. (1992). Dynamics of neuronal intermediate filaments: A developmental perspective. *Cell Motility and the Cytoskeleton*, *22*(2), 81–91.

Pallari, H., Lindqvist, J., Torvaldson, E., Ferraris, S. E., & He, T. (2011). Nestin as a regulator of Cdk5 in differentiating myoblasts. *Molecular Biology of the Cell*, *22*, 1539–1549.

Park, D., Xiang, A. P., Mao, F. F., Zhang, L., Di, C. G., Liu, X. M., … Lahn, B. T. (2010). Nestin is required for the proper self-renewal of neural stem cells. *Stem Cells*, *28*(12), 2162–2171.

Perrot, R., Berges, R., Bocquet, A., & Eyer, J. (2008). Review of the Multiple Aspects of Neurofilament Functions , and their Possible Contribution to Neurodegeneration. *Mol Neurobiol*, *38*, 27–65.

Petrovic, M., & Schmucker, D. (2015). Axonal wiring in neural development: Target-independent mechanisms help to establish precision and complexity. *Bioessays*, *37*(Sep), 996–1004.

Polleux, F., Morrow, T., & Ghosh, A. (2000). Semaphorin 3A is a chemoattractant for cortical apical dendrites. *Nature*, *404*(Apr 6), 567–573.

Poppek, D., Keck, S., Ermak, G., Jung, T., Stolzing, A., Ullrich, O., & Davies, K. J. A. (2006). Phosphorylation inhibits turnover of the tau protein by the proteasome : influence of RCAN1 and oxidative stress. *Biochem. J.*, *520*, 511–520.

Rao, M. V, Campbell, J., Yuan, A., Kumar, A., Gotow, T., Uchiyama, Y., & Nixon, R. A. (2003). The neurofilament middle molecular mass subunit carboxyl-terminal tail domains is essential for the radial growth and cytoskeletal architecture of axons but not for regulating neurofilament transport rate. *Journal of Cell Biology*, *163*(5), 1021–1031.

Reiner, O., Gdalyahu, A., Ghosh, I., Levy, T., Sapoznik, S., Nir, R., & Sapir, T. (2004). DCX's phosphorylation by not just another kinase (JNK). *Cell Cycle*, *3*(6), 747–751.

Sahlgren, C. M., Mikhailov, A., Vaittinen, S., Pallari, H., Kalimo, H., Pant, H. C., & Eriksson, J. E. (2003). Cdk5 Regulates the Organization of Nestin and Its Association with p35. *Molecular and Cellular Biology*, *23*(14), 5090–5106.

Sahlgren, C. M., Pallari, H.-M., He, T., Chou, Y.-H., Goldman, R. D., & Eriksson, J. E. (2006). A nestin scaffold links Cdk5/p35 signaling to oxidant-induced cell death. *The EMBO Journal*, *25*(20), 4808–4819.

Sakakibara, A., & Hatanaka, Y. (2015). Neuronal polarization in the developing cerebral cortex. *Frontiers in Neuroscience*, *9*(April), 1–10.

Sapir, T., Horesh, D., Caspi, M., Atlas, R., Burgess, H. a, Wolf, S. G., … Reiner, O. (2000). Doublecortin mutations cluster in evolutionarily conserved functional domains. *Human Molecular Genetics*, *9*(5), 703–712.

Schaar, B. T., Kinoshita, K., & McConnell, S. K. (2004). Doublecortin Microtubule Affinity Is Regulated by a Balance of Kinase and Phosphatase Activity at the Leading Edge of Migrating Neurons. *Neuron*, *41*(2), 203–213.

Shah, K., & Lahiri, D. K. (2014). Cdk5 activity in the brain - multiple paths of regulation. *Journal of Cell Science*, *127*(Pt 11), 2391–2400.

Shea, T. B., & Beermann, M. L. (1999). Neuronal intermediate filament protein alpha-internexin facilitates axonal neurite elongation in neuroblastoma cells. *Cell Motility and the Cytoskeleton*, *43*(4), 322–333.

Shea, T. B., Beermann, M. L., & Fischer, I. (1993). Transient Requirement for Vimentin in Neuritogenesis : Intracellular Delivery of Anti-Vimentin Antibodies and Antisense Oligonucleotides Inhibit Neurite Initiation But Not Elongation of Existing Neurites in Neuroblastoma. *Journal of Neuroscience Research*, *76*, 66–76.

Shin, E., Kashiwagi, Y., Kuriu, T., Iwasaki, H., Tanaka, T., Koizumi, H., … Okabe, S. (2013). Doublecortin-like kinase enhances dendritic remodelling and negatively regulates synapse maturation. *Nature Communications*, *4*(4), 1440.

Shinmyo, Y., Terashita, Y., Anh, T., Duong, D., Horiike, T., & Kawasumi, M. (2017). Folding of the Cerebral Cortex Requires Cdk5 in Upper-Layer Neurons in Gyrencephalic Mammals Article Folding of the Cerebral Cortex Requires Cdk5 in Upper-Layer Neurons in Gyrencephalic Mammals. *CellReports*, *20*(9), 2131–2143.

Shmueli, A., Gdalyahu, A., Sapoznik, S., Sapir, T., Tsukada, M., & Reiner, O. (2006). Site-specific dephosphorylation of doublecortin (DCX) by protein phosphatase 1 (PP1). *Molecular and Cellular Neuroscience*, *32*(1–2), 15–26.

Shupp, A., Casimiro, M. C., & Pestell, R. G. (2017). Biological functions of CDK5 and potential CDK5 targeted clinical treatments. *Oncotarget*, *8*(10), 17373–17382.

Singh, S. a, Winter, D., Bilimoria, P. M., Bonni, A., Steen, H., & Steen, J. a. (2012). FLEXIQinase, a mass spectrometry–based assay, to unveil multikinase mechanisms. *Nature Methods*, *9*(5), 504–508.

Su, P.-H., Chen, C.-C., Chang, Y.-F., Wong, Z.-R., Chang, K.-W., Huang, B.-M., &

Yang, H.-Y. (2013). Identification and cytoprotective function of a novel nestin isoform, Nes-S, in dorsal root ganglia neurons. *The Journal of Biological Chemistry*, *288*(12), 8391–8404.

Szaro, B. E. N. G., Grant, P., Lee, V. M., & Gainer, H. (1991). Inhibition of Axonal Development After Injection of Neurofilament Antibodies Into a Xenopus Zaeuis Embryo. *Journal of Comparative Neurology*, *585*, 576–585.

Tamariz, E., Varela-echavarría, A., & Greer, C. A. (2015). The discovery of the growth cone and its influence on the study of axon guidance. *Frontiers in Neuroanatomy*, *9*(May), 1–9.

Tanaka, T., Serneo, F. F., Higgins, C., Gambello, M. J., Wynshaw-Boris, A., & Gleeson, J. G. (2004). Lis1 and doublecortin function with dynein to mediate coupling of the nucleus to the centrosome in neuronal migration. *The Journal of Cell Biology*, *165*(5), 709–721.

Tanaka, T., Serneo, F. F., Tseng, H. C., Kulkarni, A. B., Tsai, L. H., & Gleeson, J. G. (2004). Cdk5 Phosphorylation of Doublecortin Ser297 Regulates Its Effect on Neuronal Migration. *Neuron*, *41*(2), 215–227.

Tsai, L. H., Delalle, I., Caviness, V. S., Chae, T., & Harlow, E. (1994). P35 Is a Neural-Specific Regulatory Subunit of Cyclin-Dependent Kinase 5. *Nature*.

Tsukada, M., Prokscha, A., & Eichele, G. (2006). Neurabin II mediates doublecortin-dephosphorylation on actin filaments. *Biochemical and Biophysical Research Communications*, *343*(3), 839–847.

Tsukada, M., Prokscha, A., Oldekamp, J., & Eichele, G. (2003). Identification of neurabin II as a novel doublecortin interacting protein. *Mechanisms of Development*, *120*(9), 1033–1043.

Tsukada, M., Prokscha, A., Ungewickell, E., & Eichele, G. (2005). Doublecortin association with actin filaments is regulated by neurabin II. *The Journal of Biological Chemistry*, *280*(3), 11361–11368.

Uchida, A., & Brown, A. (2004). Arrival , Reversal , and Departure of Neurofilaments at the Tips of Growing Axons. *Molecular Biology of the Cell*, *15*(September), 4215–4225.

Vitriol, E. a., & Zheng, J. Q. (2012). Growth Cone Travel in Space and Time: The Cellular Ensemble of Cytoskeleton, Adhesion, and Membrane. *Neuron*, *73*(6), 1068–1080.

W. Lin, B. S. (1995). Neurofilaments Help maintain Normal Morphologies and Support Elongation of Neurites in Xenopus laevis Cultured Embryonic Spinal Cord Neurons. *The Journal of Neuroscience*, *15*(December), 8331–8344.

Walker, K. L., Yoo, H. K., Undamatla, J., & Szaro, B. G. (2001). Loss of neurofilaments alters axonal growth dynamics. *The Journal of Neuroscience : The Official Journal of the Society for Neuroscience*, *21*(24), 9655–9666.

Wang, L., Ho, C., Sun, D., Liem, R. K. H., & Brown, A. (2000). Rapid movement of axonal neurofilaments interrupted by prolonged pauses. *Nature Cell Biology*, *2*(March), 137–141.

Wang, X., Sterne, G. R., & Ye, B. (2014). Regulatory mechanisms underlying the differential growth of dendrites and axons. *Neuroscience Bulletin*, *30*(4), 557–568.

Women, A. G., Yat-, S., Transplantation, O., Affiliated, T. F., Modification, P., Sciences, M., & Hospital, C. (2017). A Nestin – Cyclin-Dependent Kinase 5 – Dynamin-Related Protein 1 Axis Regulates Neural Stem / Progenitor Cell Stemness via a Metabolic Shift. *Stem Cells*, *36*, 589–601.

Xie, Z., Samuels, B. A., & Tsai, L. H. (2006). Cyclin-dependent kinase 5 permits efficient cytoskeletal remodeling - A hypothesis on neuronal migration. *Cerebral Cortex*, *16*, 64–68.

Yabe, J. T., Chan, W. K. H., Wang, F. S., Pimenta, A., Ortiz, D. D., & Shea, T. B. (2003). Regulation of the Transition From Vimentin to Neurofilaments During Neuronal Differentiation. *Cell Motility and the Cytoskeleton*, *56*(March), 193–205.

Yamada, K. M., Spooner, B. S., & Wessells, N. K. (1970). Axon Growth: Roles of Microfilaments and Microtubules. *Proceedings of the National Academy of Sciences*, *66*(4), 1206–1212.

Yamamoto, N., Tamada, A., & Murakami, F. (2003). Wiring of the brain by a range of guidance cues. *Progress in Neurobiology*, *68*(Dec), 393–407.

Yang, J., Dominguez, B., de Winter, F., Gould, T. W., Eriksson, J. E., & Lee, K.-F. (2011). Nestin negatively regulates postsynaptic differentiation of the neuromuscular synapse. *Nature Neuroscience*, *14*(3), 324–330.

Yap, C. C., Digilio, L., Kruczek, K., Roszkowska, M., Fu, X., Liu, J. S., & Winckler, X. B. (2018). A dominant dendrite phenotype caused by the disease-associated G253D mutation in doublecortin (DCX) is not due to its endocytosis defect. *Journal of Biological Chemistry*, *293*(12), 18890–18902.

Yap, C. C., Digilio, L., Mcmahon, L., Roszkowska, M., Bott, C. J., Kruczek, K., & Winckler, X. B. (2016). Different Doublecortin (DCX) Patient Alleles Show Distinct Phenotypes in Cultured Neurons. *Journal of Biological Chemistry*, *291*(52), 26613–26626.

Yap, C. C., Vakulenko, M., Kruczek, K., Motamedi, B., Digilio, L., Liu, J. S., & Winckler, B. (2012). Doublecortin (DCX) mediates endocytosis of neurofascin independently of microtubule binding. *The Journal of Neuroscience : The Official Journal of the Society for Neuroscience*, *32*(22), 7439–7453.

Yuan, A., & Rao, M. V. (2012). Neurofilaments at a glance. *J Cell Sci*, *125*(14), 3257–3263.

Z. Xu, J. Marszalek, M. Lee, P. Wong, J. Folmer, T. Crawford, ST. Hsieh, J. Griffin, D. C. (1996). Subunit Composition of Neurofilaments Specifies Axonal Diameter. *The Journal of Cell Biology*, *133*(5), 1061–1069.

Zhang, Y., Wang, J., Huang, W., Cai, J., Ba, J., Wang, Y., … Xiang, A. P. (2018). Nuclear Nestin deficiency drives tumor senescence via lamin A/C-dependent nuclear deformation. *Nature Communications*, *9*(1), 1–14.

Zhu, Q. (1997). Delayed Maturation of Regenerating Myelinated Axons in Mice Lacking Neurofilaments. *Experimental Neurology*, *316*(148), 299–316.

Abbreviations

Cdk5- cyclin dependent kinase 5

CP- Cortical Plate

DCX- Doublecortin

DIV- Day(s) *in vitro*

EV- Empty Vector

FAK- Focal Adhesion Kinase

GC- Growth Cone

IF- Intermediate Filament

INA- α-internexin

IP- Immunoprecipitation

IUE- *In Utero* Electroporation

IZ- Intermediate Zone

KD- Kinase Dead

KO- Knockout

MAP- Microtubule Associated Protein

MT- Microtubule

NF- Neurofilament

NFL- Neurofilament Light

NFM- Neurofilament Medium

NMJ- neuromuscular junction

SPN- Spinophilin (Neurabin II)

VZ- Ventricular Zone

Figure1: Nestin specifically interacts with the CDK5 substrate doublecortin

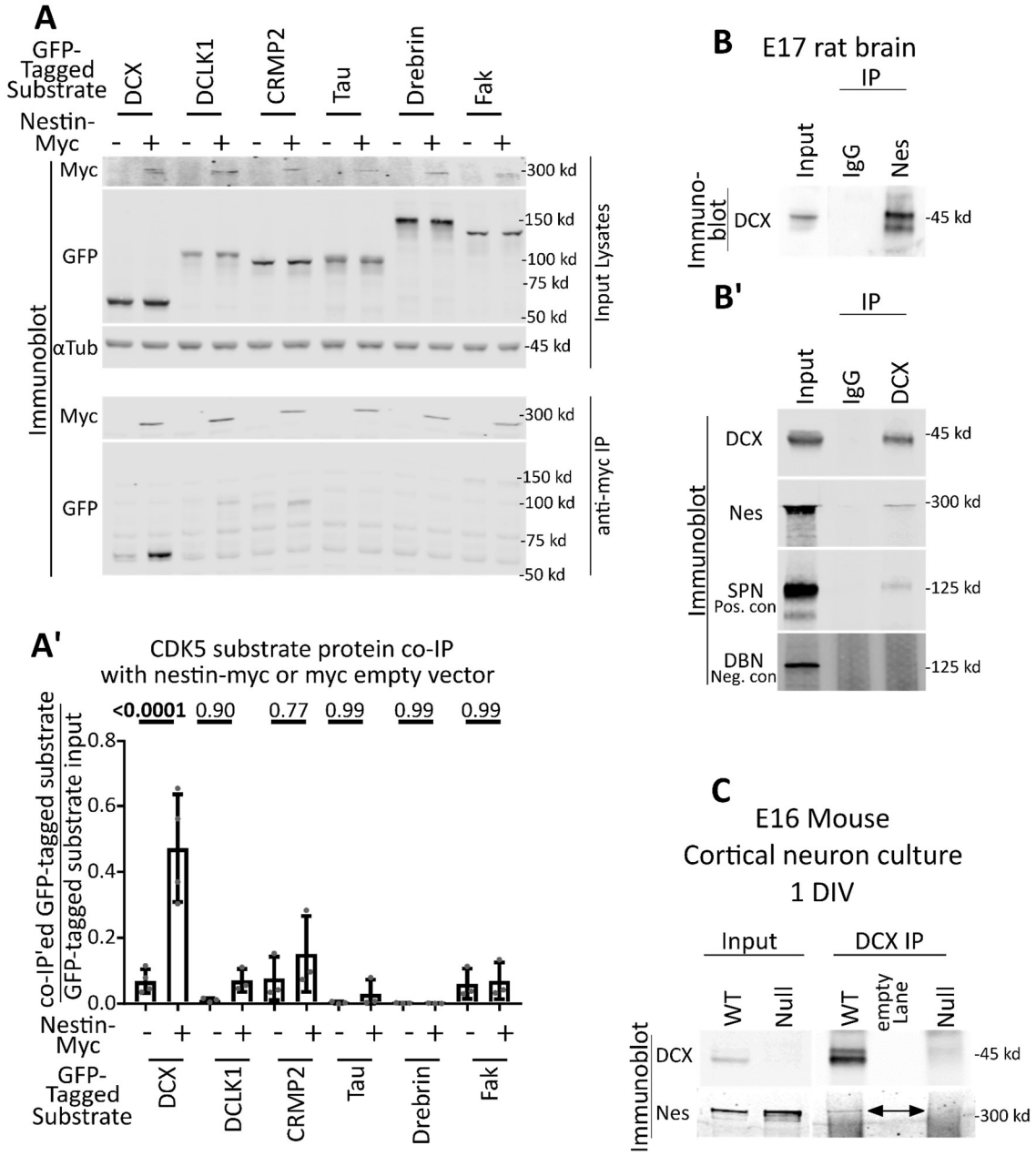

Figure2: Nestin colocalizes with DCX in the axons of newly born neurons in vitro and in vivo

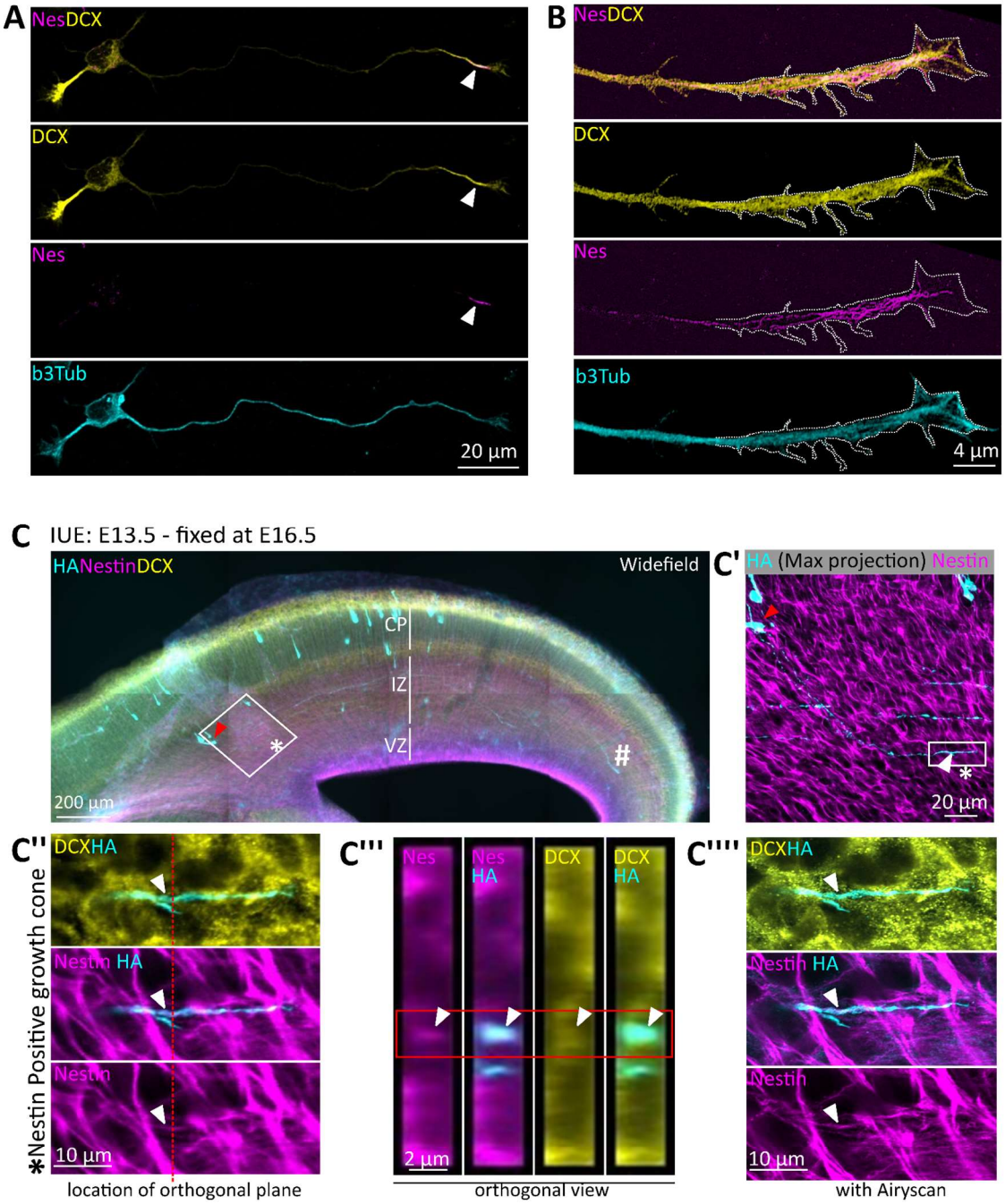

Figure3: Nestin specifically increases cdk5-dependent phosphorylation of DCX

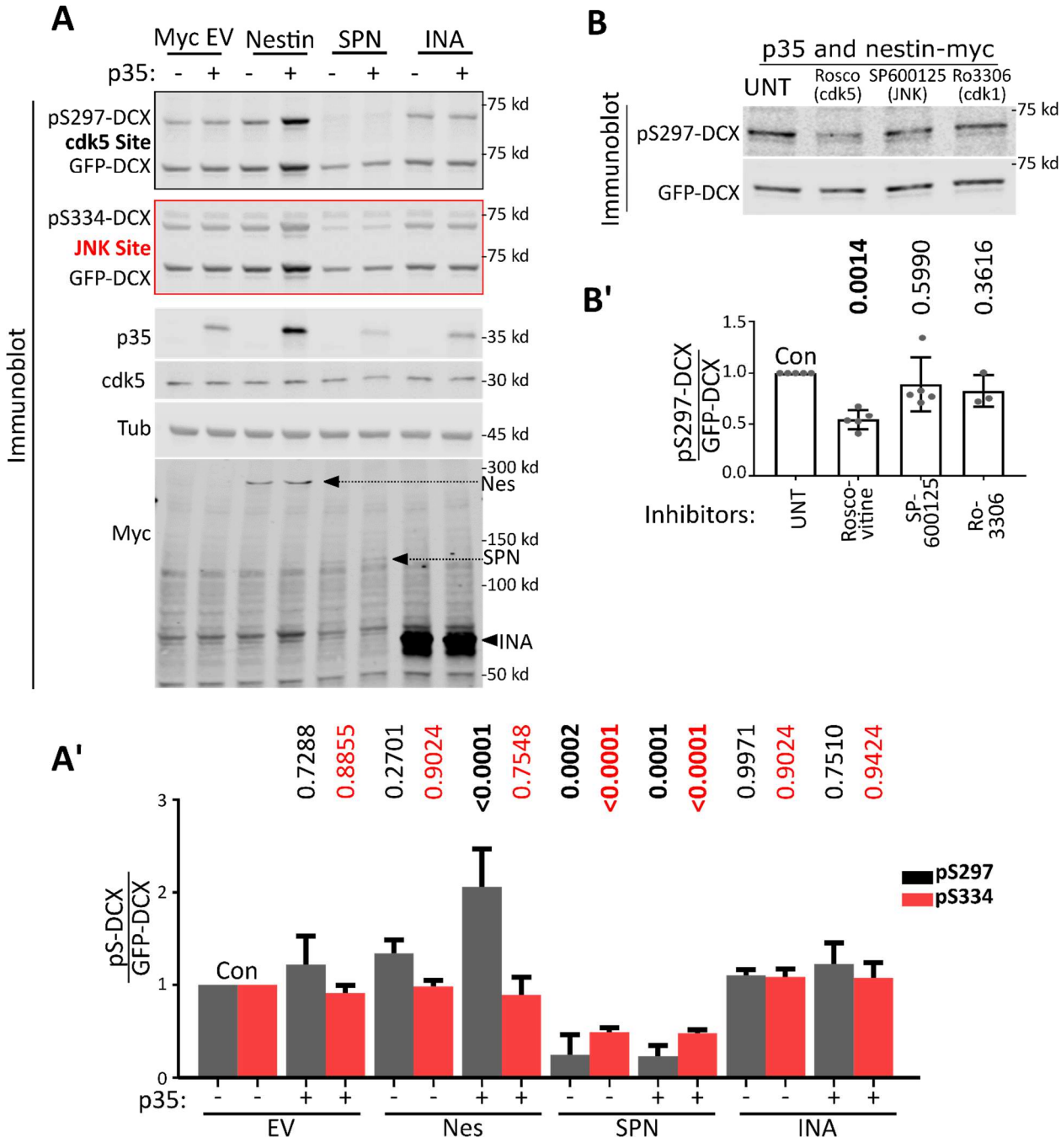

Figure4- DCX requires nestin with cdk5/p35 for significant phosphorylation, unlike other cdk5 substrates which only require cdk5/p35

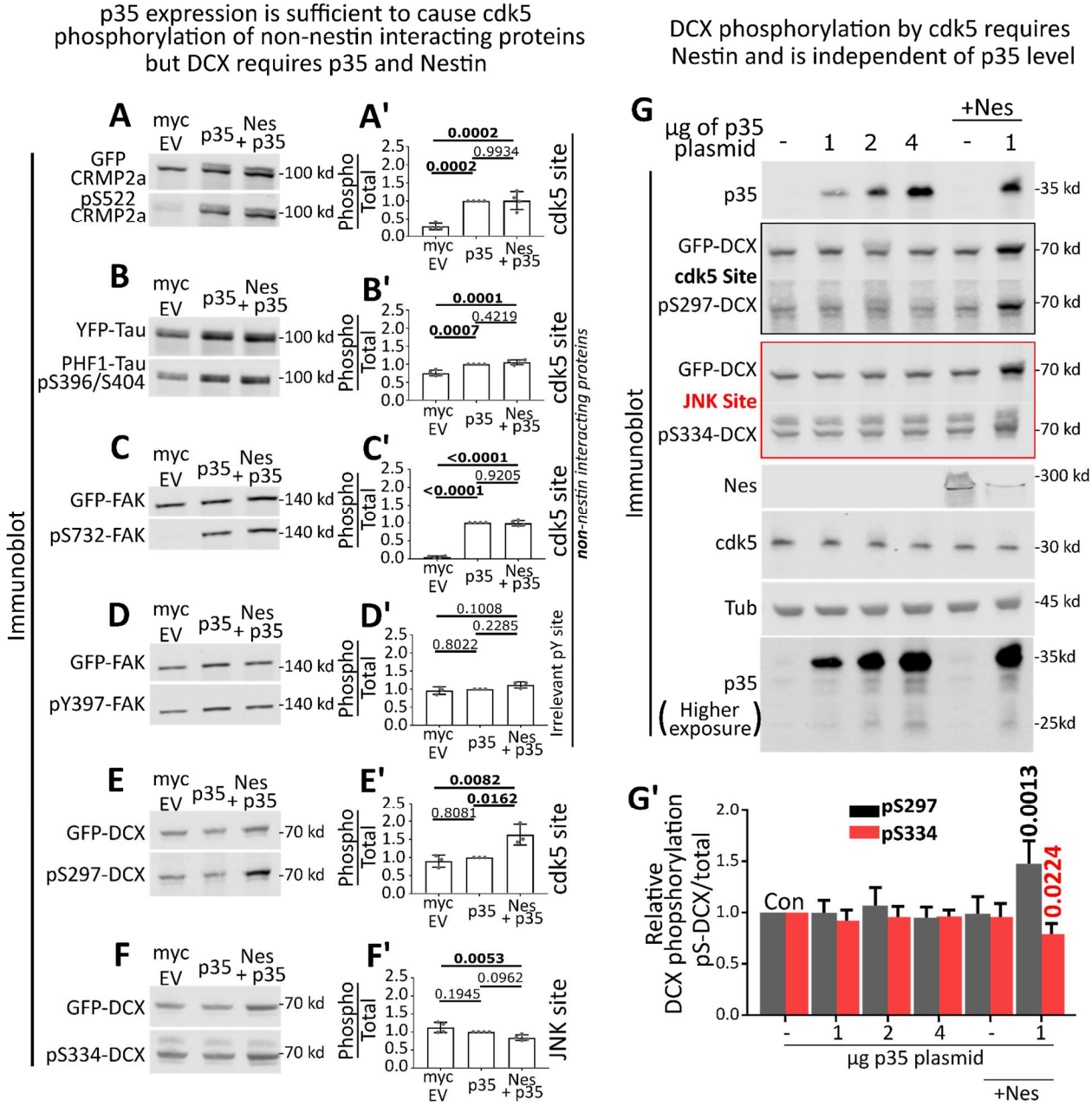

Fig5. Nestin scaffolds cdk5 and DCX to promote DCX phosphorylation

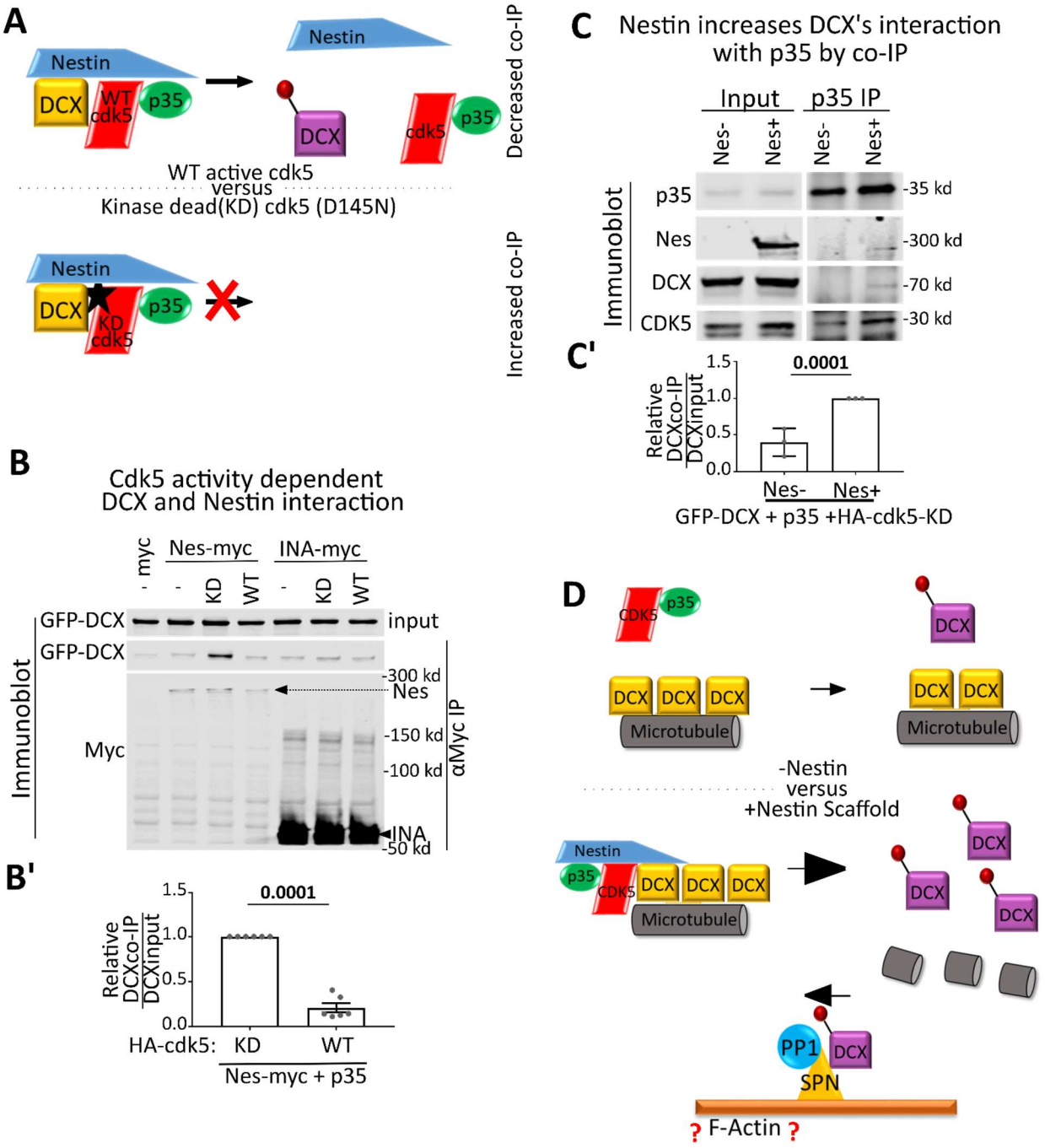

Figure6- A DCX and p35-binding deficient nestin mutant no longer affects growth cone size of DIV2 cortical neurons

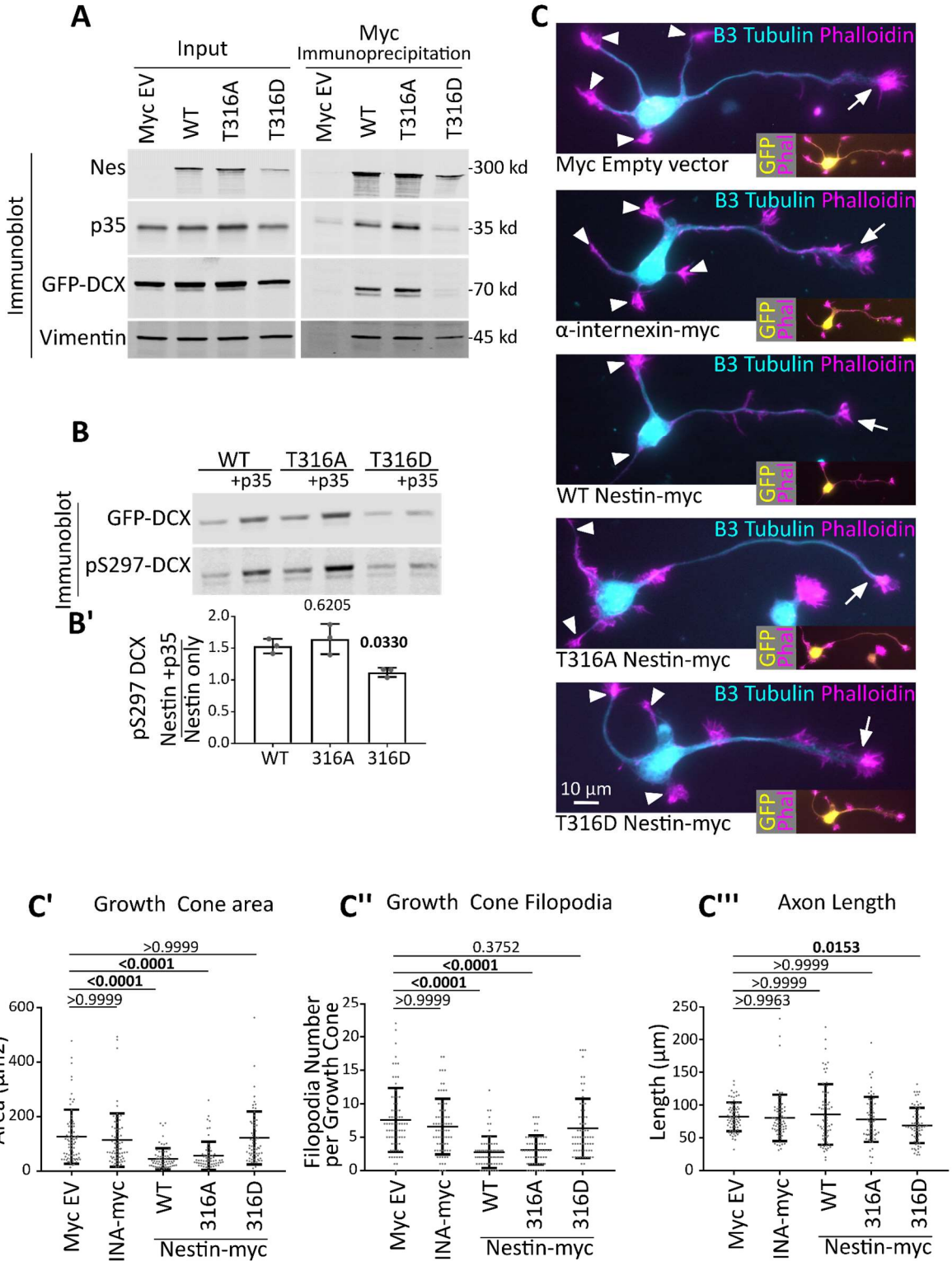

Fig7- In the absence of DCX, nestin does not cause small growth cones

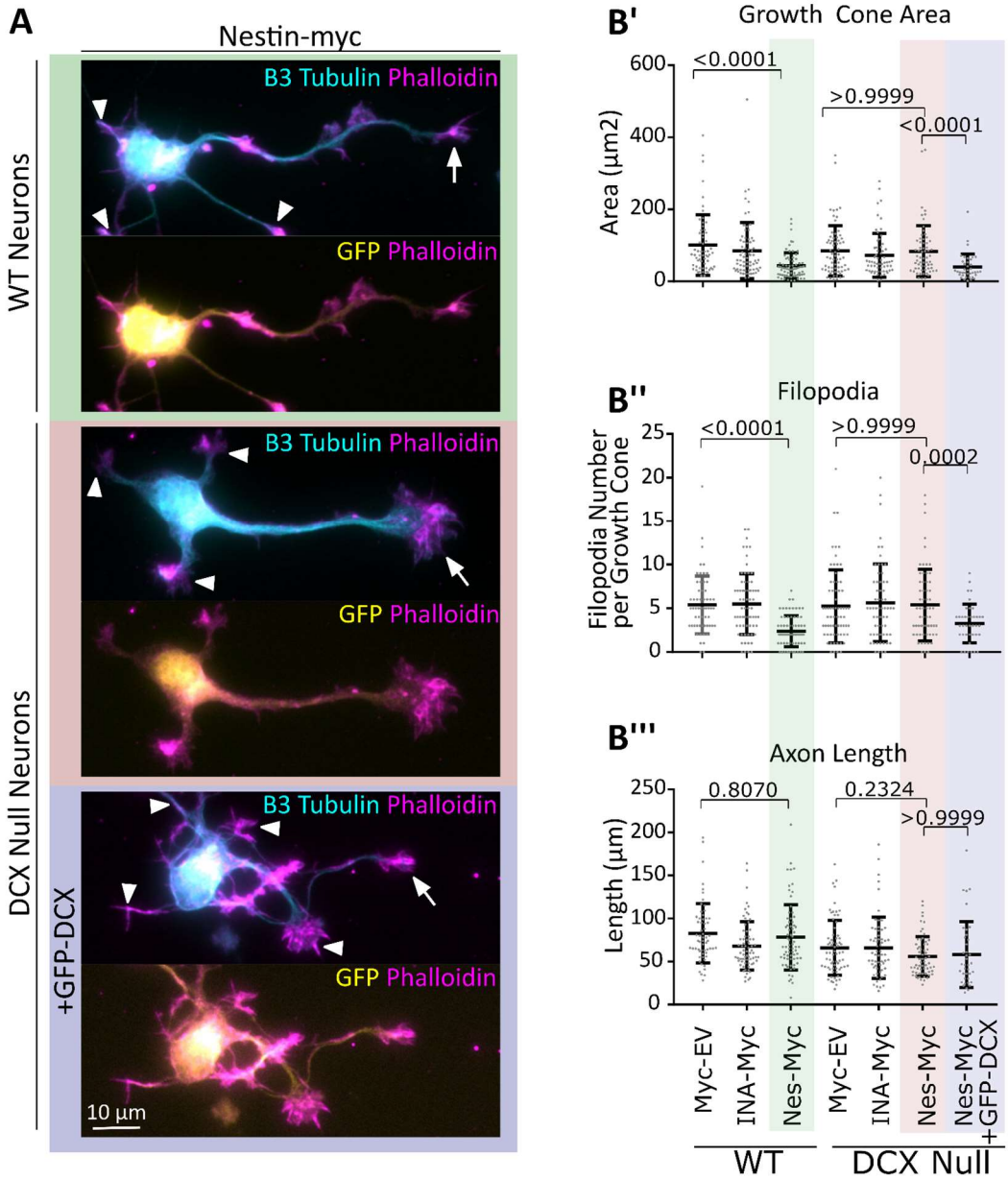

Supplement1: Nestin co-localizes with DCX-MT bundles

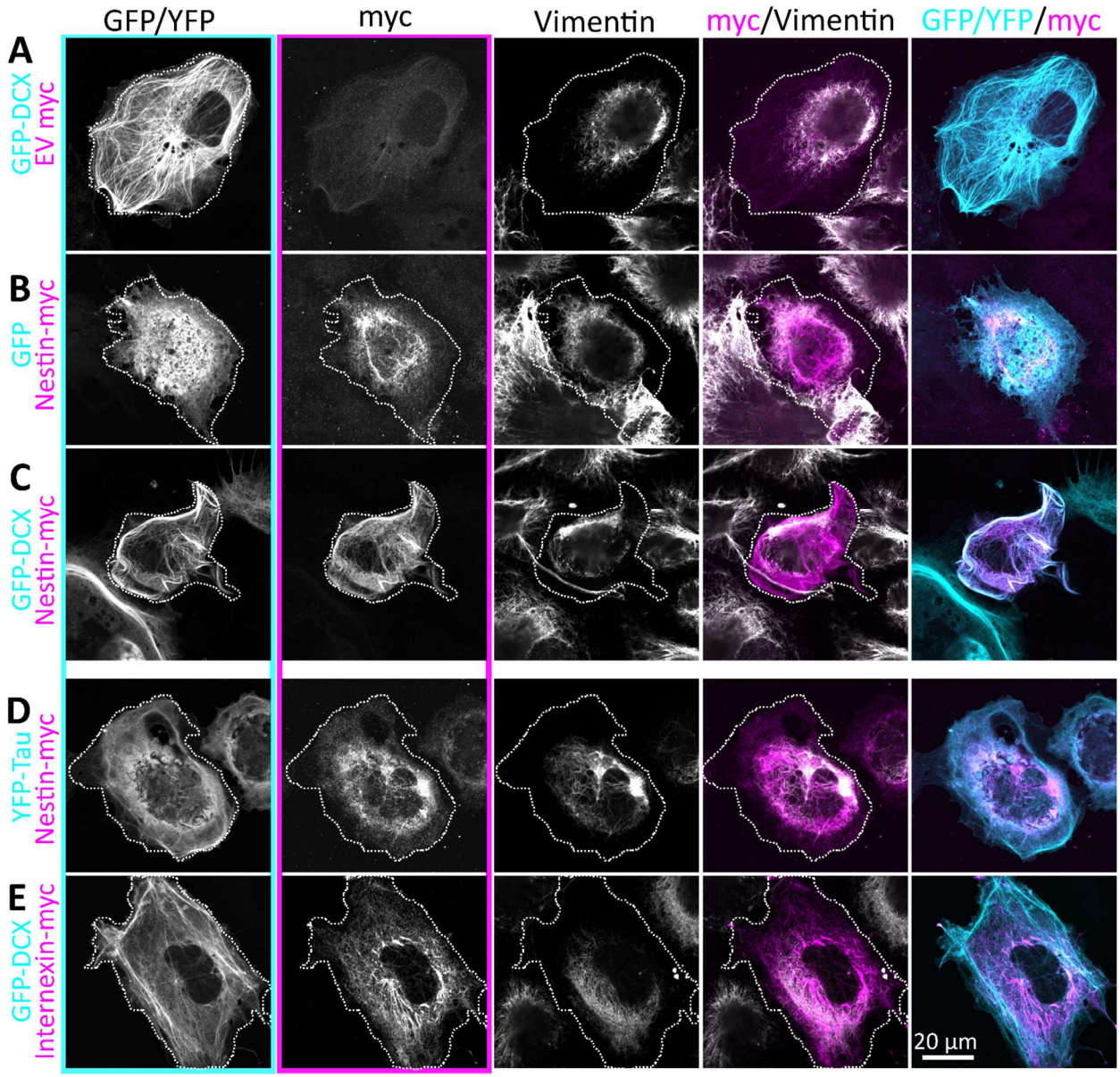

Supplement2

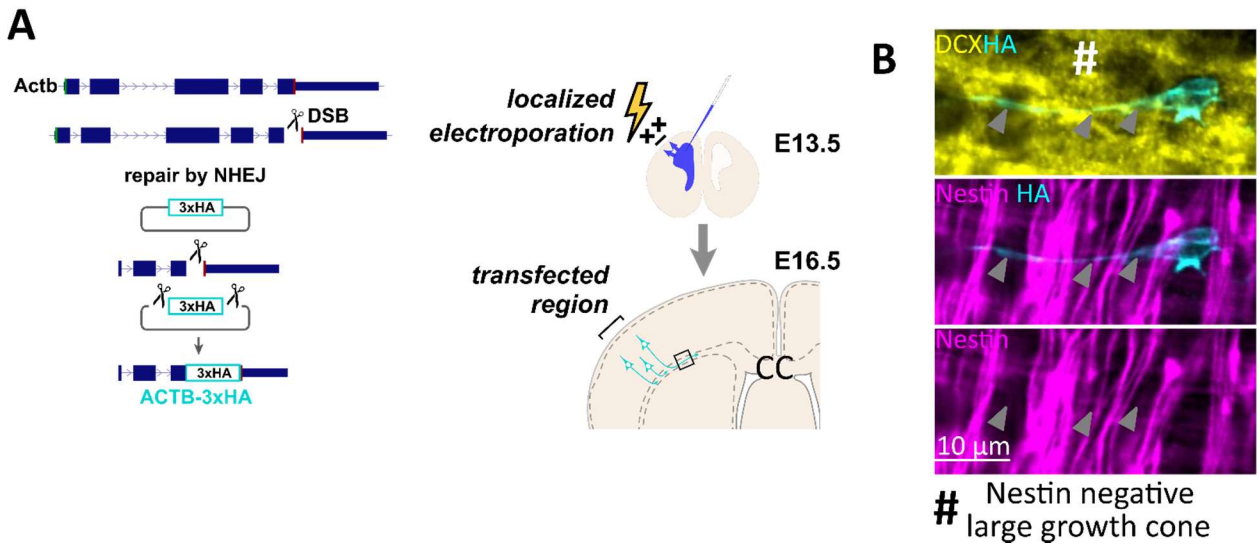

Supplement 3

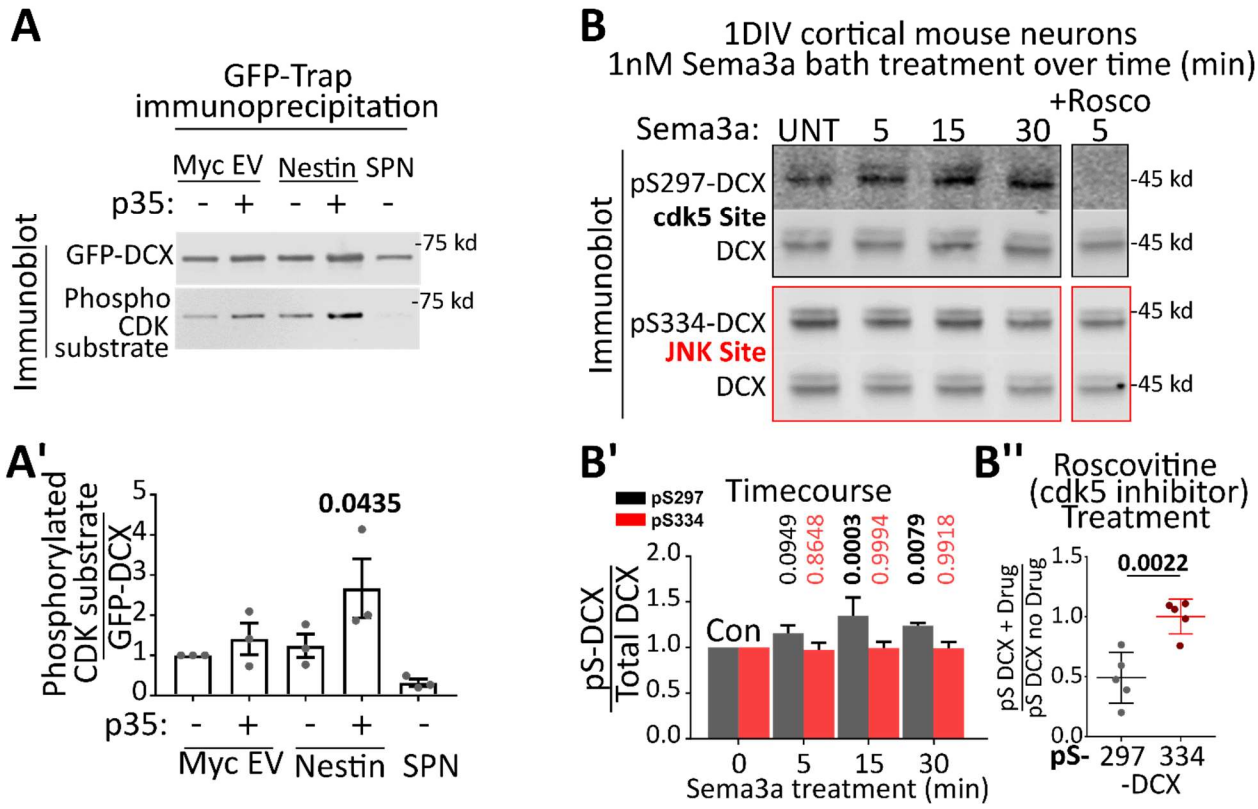
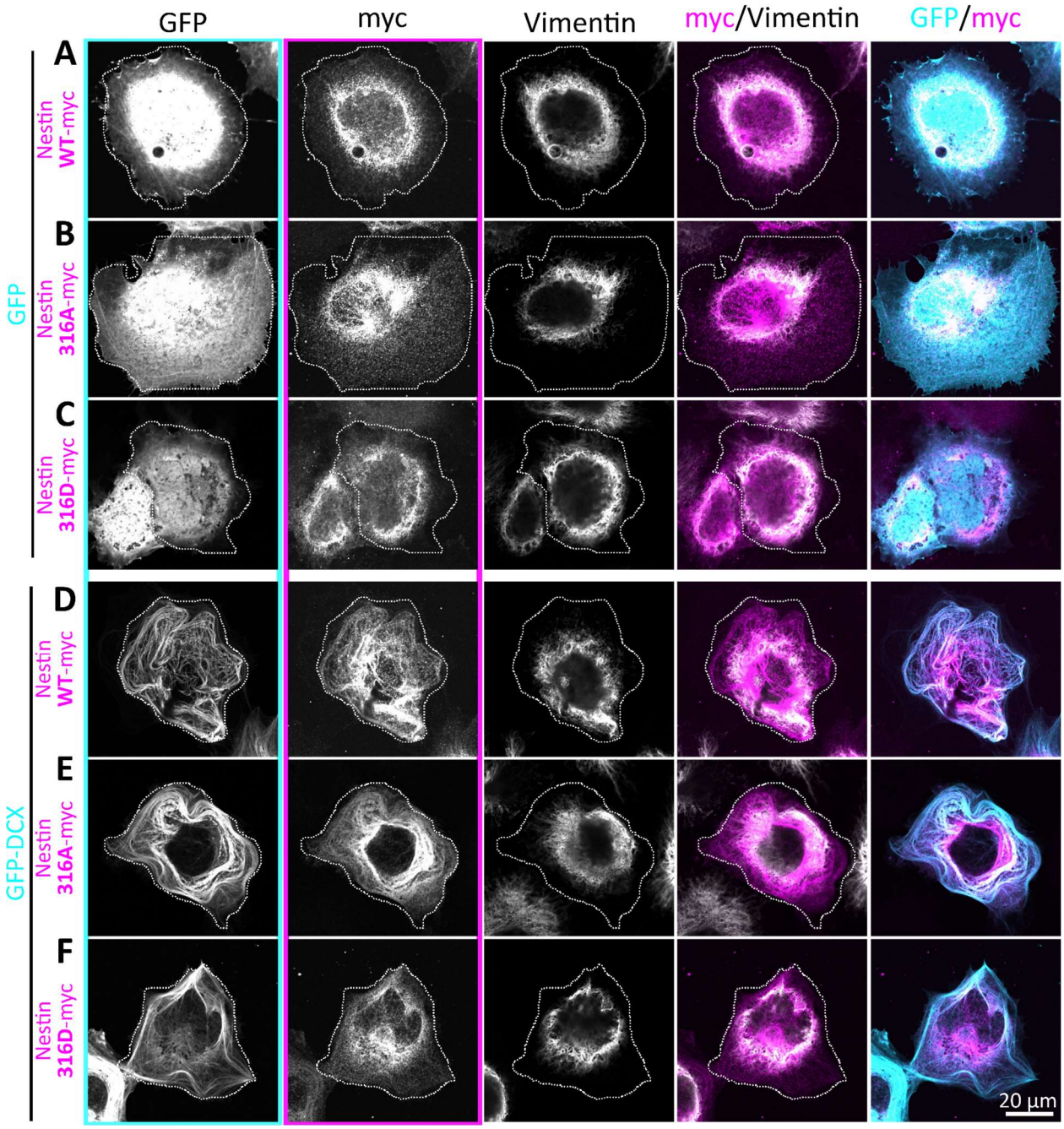
Supplement 4: Nes mutants in COS7 cells